



Ultralow platinum loading proton exchange membrane fuel cells: Performance losses and solutions

Dustin Banham^{a,*}, Jinxiang Zou^b, Sanjeev Mukerjee^c, Zihan Liu^b, Dong Yang^d, Yi Zhang^a, Ye Peng^a, Angang Dong^{b,**}

^a School of Materials Science and Energy Engineering, Foshan University, Jiangwan First Road, Foshan, 528000, Guangdong, China

^b Department of Chemistry and Shanghai Key Laboratory of Molecular Catalysis and Innovative Materials, Fudan University, Shanghai, 200433, China

^c Department of Chemistry and Chemical Biology, Northeastern University, 364 Egan Research Center, 360 Huntington Avenue, Boston, MA, 02115, USA

^d State Key Laboratory of Molecular Engineering of Polymers and Department of Macromolecular Science, Fudan University, Shanghai, 200438, China

HIGHLIGHTS

- In recent years the PGM content of PEMFCs has been greatly reduced.
- As this occurs, new performance losses are being experienced at both electrodes.
- This review discusses the observations and proposed mechanisms for these losses.
- The role of carbon support microstructure on cathode losses is also highlighted.

ARTICLE INFO

Keywords:

Proton exchange membrane fuel cells (PEMFC)
Membrane electrode assembly (MEA)
Oxygen reduction reaction (ORR)
Hydrogen oxidation reaction (HOR)
Carbon support
Electrocatalysis

ABSTRACT

In an effort to reduce the platinum group metal (PGM) content in proton exchange membrane fuel cells (PEMFCs) to a value comparable with conventional vehicles, a concerted global effort over the past decade has been made by the fuel cell community to develop high activity oxygen reduction reaction (ORR) catalysts. However, as PGM loadings in membrane electrode assemblies (MEAs) decrease below 0.125 mg/cm², it has become clear that ORR mass activity is just one of the challenges which must be overcome. At the anode, it appears that a kinetic limitation may have been reached and new research may now be required to develop hydrogen oxidation reaction (HOR) catalysts with higher turnover frequencies vs. conventional Pt. At the cathode, transport limitations have been uncovered which are related to ionomer/catalyst interactions. Recently, the critical role of the carbon support (used to disperse the PGM catalyst) on these ionomer/catalyst interactions has been revealed. Thus, rational design of carbon structures either through modification of commercial carbons or design of completely new structures, is now of utmost importance. The challenges and discoveries related to these concepts are critically analyzed in this review, along with suggestions for future research directions to help overcome the remaining hurdles.

1. Introduction

As a direct result of dedicated research on electrochemical devices over the past decade, the transition from fossil fuel-based combustion to clean energy technologies is becoming a reality in many countries. This is particularly true for motive applications, and the success of battery electric vehicles (BEVs) for passenger cars has now been well documented. However, it has also become apparent that for driving ranges

>300–400 km, a more economical solution is to hybridize batteries (high power density) with proton exchange membrane fuel cells (PEMFCs) (high energy density) [1].

The commercialization of PEMFCs has lagged that of batteries, but today, the growing momentum for PEMFCs is undeniable. Compared to lithium-ion batteries, PEMFCs demonstrate higher energy density (driving range) but lower power density (acceleration) which has made heavy duty (HD) applications such as buses an ideal entry point into the

* Corresponding author.

** Corresponding author.

E-mail addresses: dustin_banham@fosu.edu.cn (D. Banham), agdong@fudan.edu.cn (A. Dong).

<https://doi.org/10.1016/j.jpowsour.2021.229515>

Received 12 September 2020; Received in revised form 29 December 2020; Accepted 12 January 2021

Available online 3 February 2021

0378-7753/© 2021 The Authors. Published by Elsevier B.V. This is an open access article under the CC BY license (<http://creativecommons.org/licenses/by/4.0/>).

market for this technology. Additionally, as buses typically return to the same station at the end of their working shift, a ‘centralized’ refueling strategy can be used to eliminate challenges associated with deploying sufficient hydrogen refueling stations to serve a large fleet. While HD applications represent an excellent starting point, a recent survey by KPMG of ~1000 senior executives from world leading automotive original equipment manufacturers (OEMs) reports that nearly 80% absolutely or partly view PEMFCs as the long term solution to electrifying the drive train of passenger vehicles [2]. Clearly then, there is a high degree of optimism within the automotive industry for PEMFCs, but the transition from HD to passenger vehicle applications will not be trivial.

As PEMFC technology prepares for entry into the passenger vehicle market, the demands on this technology will be intensified as never before. This is particularly true for the anode and cathode catalyst layers, where the current combined platinum group metal (PGM) content is still 4–6x higher than typical catalytic converters used in conventional vehicles [3–5]. Due to the significantly lower kinetics of the oxygen reduction reaction (ORR, occurring at the cathode) vs. the hydrogen oxidation reaction (HOR, occurring at the anode), significant research effort over the past decade has been focused on developing advanced ORR catalysts. Through this work, it has become evident that a large number of advanced PGM catalysts now exist with exceptionally high ORR activity [6–9], greatly exceeding the mass activity of conventional Pt/Pt-alloy catalysts, at least when measured through rotating disc electrode testing (RDE). Furthermore, while it has been well documented that RDE-level activities do not always translate well to MEA-level activities [4,10,11], there are now several reports of successful integration of these high activity catalysts into MEAs capable of achieving the generally accepted mass activity target of 0.44 A/mg [8, 12–14].

These technological achievements, understandings, and MEA-integration activities of novel ORR catalysts have all received great attention, and there have recently been many thorough reviews covering all aspects of this work including catalyst activity, durability, and MEA performance [10,11,15,16]. Thus, it is not the goal of the present review to reiterate what has already been thoroughly discussed, and any readers interested in a ‘catalyst specific’ review are directed to one of these previously published review articles. Rather, the focus of the present review is on performance losses that are unique to ‘low loaded’ MEA designs. Specifically, significant performance limitations have been observed at both the anode and cathode of the MEA as total areal loadings are decreased to <0.125 mg/cm². While degradation of the catalyst (either anode or cathode) undoubtedly exacerbates these losses, they are observed even at ‘beginning of life’ (BOL). The mechanism(s) for these overpotentials are quite different at the anode and cathode, with the former being largely a kinetic loss and the latter being a transport phenomenon. At this stage of PEMFC development, understanding and overcoming these losses has become critically important, and thus provides the motivation for the present review.

Here, we highlight the challenges that have been observed at both the anode and cathode, and discuss opportunities to overcome them. While a brief overview of ORR catalyst development is provided, it is meant only as a refresher for anyone not familiar with the field, as many thorough reviews are already available [10,11,17]. At the cathode, a particular focus on the somewhat underappreciated role of the carbon support (which is used to disperse the PGM catalyst) in overcoming cathode losses is discussed, along with a brief discussion of advanced carbon structures which may provide opportunities in the near future to unlock previously unattainable performance at ultra-low PGM loadings.




2. Performance challenges at ultralow PGM loadings

2.1. PGM catalysts

In order to catalyze the HOR at the anode and the ORR at the

Table 1

Approximate PGM content in commercial PEMFC applications based on currently achievable Pt loadings.

Stack Power	Application	Example	Total Pt Content	Total Cost from Pt (USD) ^a
1–25 kW	<ul style="list-style-type: none"> • Portable Power • Scooters 		~0.3–8 g	\$ 10–240
25–75 kW	<ul style="list-style-type: none"> • Range extender • Bus • Transport truck 		~8–25 g	\$ 240–750
>75 kW	<ul style="list-style-type: none"> • Passenger vehicle 		~25–35 g	\$ 750–1050

^a Cost based on current Pt price of ~30 USD/g [19].


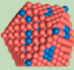
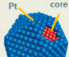


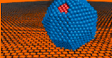
cathode, PGM catalysts are required at both electrodes. The loading of these catalysts is most commonly reported as mgPGM/cm². For commercial applications today, the typical total loading of PGMs (anode + cathode) is ~0.25–0.35 mg/cm² [4,18]. Table 1 illustrates what this translates to in terms of total PGM content for a variety of applications. It should be noted that the reason bus applications are shown as having lower power requirements than passenger cars is simply a reflection of the current state of commercialization of these two applications. The majority of commercial PEMFC stacks for bus applications have been sold in China, where the targeted power was initially set at ~50 kW. This relatively low power requirement is part of China’s staged approach to PEMFC deployment, where the subsidy program is used to encourage steady growth in PEMFC technology by continually increasing the minimum stack power that is eligible for government support. Conversely, the two currently commercial PEMFC-powered passenger cars (Toyota Mirai and Hyundai Nexo) rely on fuel cell stacks with power output closer to 100 kW.

While the data in Table 1 is highly encouraging, achieving the targeted total (anode + cathode) areal Pt loadings of <0.125 mg/cm² is not possible with conventional carbon supported Pt catalysts (Pt/C). As ~80% of the total PGM loading is typically at the cathode, an MEA loading of 0.125 mg/cm² would translate to ~0.1 mg/cm² PGM at the cathode, with only ~0.025 mg/cm² PGM at the anode. The sluggishness of the ORR vs. the HOR is widely acknowledged [20], and thus with these PGM loadings in mind, most of the focus in the research community was on developing new ORR catalysts with improved mass activity vs. Pt/C, with little attention paid to the anode. However, as will become clear later in this review, anode kinetics may now be an area that deserves higher attention if anode loadings of 0.025 mg/cm² are to become a reality. For now, the next section will focus on ORR catalyst activity, as there is little to discuss in terms of HOR catalyst development (with respect to activity).

2.1.1. Development of cathode catalysts with high mass activities

For nearly a decade, there has been a strong focus by materials scientists and MEA designers to achieve a PGM-mass activity of 0.44 A/mg, which was set as the United States Department of Energy (US DOE) 2017 and 2020 catalyst mass activity target. The motivation for this target is evident when examining the mass activities achievable for conventional Pt-based electrocatalysts [21]. Taking Tanaka Kikinzoku Kogyo’s TEC10E50E as an industry standard Pt/C catalyst, the mass activity (measured in an MEA) has been reported to be ~0.11 A/mg [21]. Clearly, simply decreasing the loading using the same catalyst will result in kinetic losses, which are experienced over all current densities in the MEA. The most obvious solution to this problem was to offset the 4x decrease in loading by actively developing new ORR catalysts which had

Table 2
Pipeline of the development of cathode catalysts.

Benefits: • Commercially mature	Challenges: • Low A/mg	Pt nanoparticles 	
Benefits: • Commercially mature • Improved A/mg	Challenges: • Catalyst durability	Alloy/de-alloy nanoparticles 	
Benefits: • High A/mg • Very high ECSA	Challenges: • Scale up • Durability	Core-shell nanoparticles 	
Shaped nanocrystals 	Benefits: • Very high A/mg • Scalable	Challenges: • Stability/activity at MEA-level still not fully known	
Nanoframes 	Benefits: • Very high A/mg • Highly durable	Challenges: • Scale up • Incorporation into catalyst layers	
Hybrid catalysts 	Benefits: • High mass activity	Challenges: • Low site density • Mass transport limitations	
R&D Phase	MEA Evaluation	Stack Testing	Commercialized

4x higher activity than Pt/C. Thus ensued a challenging, but successful, pursuit of catalysts which could achieve ≥ 0.44 A/mg in an MEA [8].

Mass activity is a product of specific activity ($\mu\text{A}/\text{cm}^2$ Pt) and electrochemically active surface area (ECSA, m^2/g Pt) as shown in Eq. 1

$$\text{Mass Activity} \left(\frac{\text{A}}{\text{mg}} \right) = \text{ECSA} \left(\frac{\text{m}^2}{\text{g Pt}} \right) \times \text{Specific Activity} \left(\frac{\mu\text{A}}{\text{cm}^2 \text{ Pt}} \right) \times \frac{1}{100000} \quad (1)$$

It is clear from Eq. (1) that two approaches can be taken to improve activity: 1) Increase the specific surface area and 2) Increase the specific activity (turn over frequency/exchange current density). However, as will be discussed, there are limited gains to be achieved through attempting to develop smaller Pt particle sizes.

It has been repeatedly demonstrated that specific activity and ECSA are not independent variables. This is due to both a change in the dominant terminating crystal face (or Miller index) [22], and the exponential increase in edge sites as particle size decreases, leading to an overbinding of oxygen species and a dramatic decrease in specific activity [23,24]. The ‘peak’ mass activity for Pt nanoparticles has been reported to be ~ 2 nm when evaluated in nonbinding electrolytes (e.g. HClO_4) [23], vs. ~ 4 nm in strongly binding electrolytes (e.g. H_2SO_4) [25], likely as result of the different interactions of weakly vs. strongly binding anions on the terminating crystal face of the particle. Regardless of these points, it is clear that decreasing particle size is not a viable solution to increasing mass activity at this stage of development. Thus, research on increasing mass activity must primarily be focused on increasing the inherent activity (exchange current density) of PGM based catalysts.

With more than a decade of research focused on approaches to increase turnover frequency, it is not surprising that there are now many strategies and synthetic approaches that have been developed. Broadly,

these strategies have been based on either the ‘ligand effect’ or the ‘lattice strain’/‘surface strain’ effect [26]. These concepts have been thoroughly reviewed [27–29], and here we present only a brief overview.

The ligand effect emanates from the juxtaposition of dissimilar transition elements within a lattice framework eliciting changes in the overall density of states (aka d-band vacancy). Such substitutional alloy formation has an inherent associated lattice strain effect associated with compression or expansion of the lattice. This is akin to predictable lattice parameter variations as a function of the degree of substitution of one metal into another in accordance with Vegard’s law [30]. Surface strain on the other hand is a function of both the substitutional effects of alloy formation and the effect of small particle size (< 2.5 nm [31]) containing a fair degree of low coordination planes on the surface. This can have a profound impact on ORR activity, with a compressive strain of $\sim 1\%$ resulting in $> 300\%$ increase in turn over frequency [27,32]. However, as pointed out earlier [33], lowering of particle size below 2.5 nm has an exponential effect on electronic states which for most charge transfer steps is increasingly detrimental for both oxidative and reductive charge transfer steps. Hence indiscriminate reduction of particle size below 2.5 nm is not a useful strategy. Instead, surface strain is introduced/observed in core-shell catalysts, where the dissimilar lattice structure of the core induces strain effects on the Pt shell. To prevent dissolution of the core, Pt shells of ≥ 2 monolayers may be required, as was recently highlighted for a novel Pt shell/TiWN core catalyst [34]. However, to maximize the benefit of core-shell structures the shell is typically $< 3\text{--}4$ monolayers thick [35]. Thus, with such thin shells typically targeted, in the majority of instances it is likely that both strain and ligand effects are simultaneously present and are not mutually exclusive.

Most studies on achieving high turnover frequency have focused on designing highly ordered structures which are carefully tuned, targeting a specific crystallographic orientation. While these studies are appealing

on a fundamental level [36–38], it is challenging to maintain the desired shape in an operating fuel cell, where the hot/acidic environment in combination with a relatively large potential window renders these structures unstable [39]. Fortunately, it has been reported that high turnover frequencies can also be achieved through a rather unintuitive approach: introducing structural *disorder*. This approach has actually lead to some of the highest ever reported ORR mass activities, such as the jagged Pt nanowires [6] (RDE-based activity of 13.6 A/mg). In recent work by Chattot et al. [40], the authors introduced surface distortion (SD) as a new descriptor for ORR activity of both ordered and disordered catalysts. SD can be obtained through analyzing the Rietveld refinement of the wide angle X-ray scattering measurements, and was used by the authors to study a series of ordered and disordered PtNi catalysts. In addition to introducing SD as a descriptor of ORR activity, a key finding from this work was that catalyst strategies based on disordered structures ($SD > 0$) have greater potential to become commercially viable vs. highly ordered catalysts ($SD = 0$) as disordered structures are far more stable in a PEMFC environment. Another intriguing advantage of disordered catalysts is that they have a multiplicity of active sites which theoretically allows for optimization towards multiple electrochemical reactions (e.g. ORR and OER) with the same material.

Lastly, it is also important to briefly discuss the critical role of anion binding on measured ORR activities. Based on numerous RDE measurements [41–43], it is now known that the ORR activity of the low index Pt planes (Pt (111), Pt (110), Pt (100)) are not equal, with the exact sequencing depending on whether the activity measurement is performed in the presence of a strongly (e.g. HSO_4^-) or weakly (e.g. ClO_4^-) adsorbing anion [42,43]. While it is seemingly intuitive that changing the terminating Pt crystal face will impact the measured ORR activity, translating this into useful catalyst design information requires some consideration. One important point is whether the data obtained in HClO_4 or H_2SO_4 will be more representative of MEA data. In this case, the question is really whether or not the ionomer can be considered ‘strongly binding’. Interestingly, there have been directly opposing reports in literature regarding this issue. Electrochemical mass activity testing of Pt/C catalyst in HClO_4 appeared to give results closer to those obtained in an MEA (vs. RDE testing in H_2SO_4), leading some authors to conclude that the ionomer in the electrode must also be ‘non adsorbing’ [21]. This appeared to be in direct conflict with spectroscopic studies, which provided strong evidence for the adsorption of ionomer (through the SO_3^- anion) on the Pt surface [44], and electrochemical evidence showing that the specific activity of bulk polycrystalline Pt electrodes, as well as supported Pt nanoparticles, decreases in the presence of an ionomer film [45,46]. The answer to this seeming dichotomy may result from the previously underappreciated role of carbon nanostructure on Pt activity. When supported platinum nanoparticles are housed inside pores of $< \sim 10$ nm, they are no longer in direct contact with the sulfonate groups in the catalyst layer [4], and thus may demonstrate a specific activity closer to that obtained in HClO_4 vs. H_2SO_4 electrolytes. Thus, whether the ionomer acts as ‘binding’ or ‘non-binding’ in the cathode catalyst layer (CCL) may largely be a result of the carbon structure used to support the Pt catalyst [45]. This is a critical point, as it suggests that Pt catalysts and carbon structures should not be designed independently.

2.1.2. Current cathode catalyst types

Through focusing on turnover frequency, many novel ORR catalysts have been developed which broadly speaking can be considered as: 1) Pt-only, 2) Pt-alloy, 3) Core-shell, 4) Shape controlled, 5) Porous/Nanocage, and 6) Hybrid catalysts (Table 2). There is also of course significant work on nonprecious metal catalysts (NPMCs), which have been the focus of several previous reviews [47–49], but falls out of the scope of the present review. Catalysts 1–5 have been previously discussed in other reviews [10,11], but recently a promising new class of hybrid catalysts has emerged, formed by combining traditional NPMCs

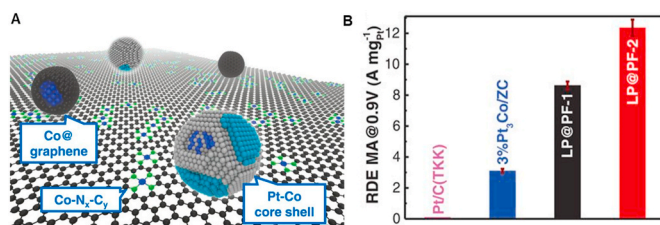


Fig. 1. (A) Schematic of the PtCo/NPMC hybrid catalyst and (B) mass activities [13], reprinted with permission from the American Association for the Advancement of Science.

with PGM catalysts, which warrants a brief discussion.

The lower material cost of NPMCs vs. PGM catalysts is likely their primary advantage (although the unique tolerance towards contamination of NPMCs [50,51] provides another promising advantage vs. PGMs). However, these catalysts still suffer in terms of low mass activity and poor stability (performance loss during galvanostatic or potentiostatic conditions [47]). As was previously discussed [47,52–54], in general there are 4 mechanisms in literature which have been proposed as reasons for the poor stability of NPMCs: 1) attack by H_2O_2 and/or free radicals [55,56] 2) dissolution of the active metal center [57], 3) protonation of active sites or protonation of N species neighboring the active sites followed by anion adsorption [58], and 4) flooding of micropores [59]. The relative importance of each of these mechanisms surely varies depending on the nature of the NPMC chemistry and microstructure, but increasingly the evidence has pointed towards mechanism 1 as being the most damaging [48,52,54,56,60]. While the active site(s) of NPMCs has been the source of much debate in the NPMC community (Fe [61], N [62], and/or carbon defect sites [63,64]), the most promising class of NPMCs have been the Fe/N/C variety. In recent work by Zelenay et al. [65], direct evidence of single atom Fe centers was provided. The authors were also able to demonstrate the importance of these sites through quantum chemical modelling, which indicated that edge-hosted sites were responsible for the majority of the ORR activity that was observed. Advances such as these have enabled NPMC to begin penetrating the commercial market [66], but the mass activity and stability are still far below what is required for most commercial applications.

For PGM based catalysts, the only challenge is related to cost. It is therefore not surprising that several groups have started looking at combining these two classes to a hybrid catalyst which can overcome the individual weakness of each respective catalyst, but the strategy of how to combine PGM and NPMCs does require some consideration. A strength of NPMCs is their atomically dispersed active sites, and to preserve this, atomically dispersed Pt sites may initially seem appealing. However, for Pt it is known that for the ORR to occur, a minimum ‘ensemble’ of Pt atoms is required, and that as a ‘single atom’ site is approached, the 2e-reduction to H_2O_2 becomes favorable [67–71] (this may be different for the HOR, where atomically dispersed Pt may show some promise [72]). Despite this concern, in recent work Zheng et al. [73] did exactly this by grafting Pt atoms directly to conventional Fe–N₄ active sites. Surprisingly, the resulting catalyst showed very little improvement in ORR activity, but was significantly more stable than the baseline NPMC. This was proposed to be due to the Pt atoms inhibiting the formation of H_2O_2 , but in light of what is known regarding H_2O_2 generation at single atomic Pt sites, the mechanism seems unclear. In a related strategy, Chong et al. [13] developed a hybrid catalyst by forming PtCo nanoparticles on a NPMC matrix. This catalyst demonstrated exceptionally high mass activity at the MEA level (~ 1.8 A/mg) as well as good durability during voltage cycling (Fig. 1).

While these results are certainly promising, this catalyst showed insufficient high current density performance for commercial applications. This is likely related to the limited site density of this catalyst vs. conventional PGM catalysts. The total Pt content of this catalyst is

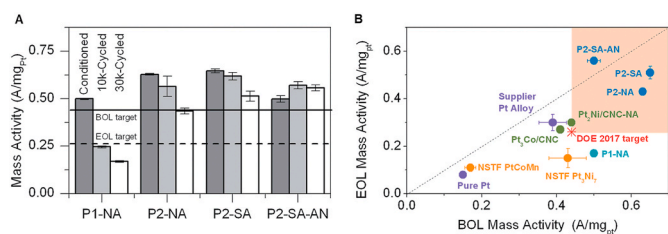


Fig. 2. (A) Mass activities reported from MEA testing of de-alloyed PtNi core-shell catalysts and (B) a comparison of mass activity at before and after voltage cycling [8], reprinted with permission from the Royal Society of Chemistry.

reported to be < 3 wt%, which is ~ 15 x lower than conventional commercial PGM catalysts, but the mass activity of 1.8 A/mg is ~ 5 x higher than conventional PGM/PGM-alloy catalysts [74]. Thus, to achieve the same current density (A/cm² MEA) as a conventional PGM alloy at typical loadings of ~ 0.2 mg/cm², this new hybrid catalyst would require a catalyst layer ~ 3 x as thick as the conventional PGM layer which would result in high mass transport losses and thus reduce the maximum achievable current density. To decrease catalyst layer thickness, an increase in both Pt and non-precious active sites would be required as the impressive activity of this catalyst relies on intimate contact between the Pt and the non-precious active site [13]. In this case, the largest bottleneck will almost certainly be the ability to increase non-precious active sites, which has historically been quite challenging [75,76]. Therefore, this class of catalyst will likely suffer from low MEA performance until further advances can be achieved in increasing non-precious active site densities. This is an important point, as too often the focus is placed exclusively on mass activity, when for commercial applications, the performance at high current density is arguably more important. Thus, it is likely that the primary challenge moving forward for hybrid catalysts will be similar to that of NPMCs; namely, to maintain the promising activity and durability while increasing total site density.

2.1.3. Presently achievable MEA mass activities

It is now widely acknowledged that RDE-level mass activities do not translate directly into MEA-level mass activities. Therefore, when judging the success of recent ORR catalyst development, it is important to focus on what has been achieved at the MEA-level. However, a survey of the literature quickly reveals that there are in fact relatively few reports of mass activity at the MEA-level. There are a variety of reasons for this, including a lack of expertise, large capital investment required to perform MEA testing, and the requirement of gram level quantities of catalyst to prepare the MEA catalyst layer. Nonetheless, there have been several reports of catalysts exceeding the target of >0.44 A/mg based on MEA testing [8,12–14]. A particularly promising variety are the de-alloyed PtNi core-shell structures developed by Han et al. [8] In what is one of only a few thorough MEA-level studies of advanced ORR catalysts, the authors report record high mass activities, which exceed the stated target of 0.44 A/mg (Fig. 2).

While such reports are still not widely available, the promising progression of ORR catalysts (Table 2) combined with these reported MEA-level mass activities give great hope that materials-level catalyst technology will not be a long term bottleneck for PEMFC commercialization. However, as these novel ORR catalysts are increasingly advanced past RDE testing and are incorporated into MEAs with ultra low PGM loadings, the entire PEMFC community is now being confronted with previously unexpected challenges that cannot be detected without MEA testing.

2.2. Anode performance losses at low PGM loadings

Until recently, kinetic performance losses at the anode of a PEMFC have been largely ignored, and rightfully so considering there is nearly no impact on performance as anode loadings are decreased from 0.1 to

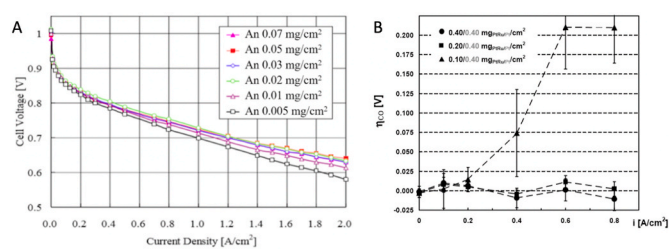


Fig. 3. (A) Polarization curves at various anode loadings [77], reprinted with permission from the Electrochemical Society. (B) Effect of anode loading on CO tolerance [78], reprinted with permission from Elsevier.

0.05 mg/cm². However, below this loading, performance losses have been reported [77,78] (Fig. 3A). In fact, even with a highly optimized electrode design, performance losses can be expected at loadings $\leq \sim 0.02$ mg/cm² [79]. Considering anode loadings are now being targeted at ≤ 0.025 mg/cm², it is clear that some strategies for overcoming these losses will now be necessary. This is particularly true when acknowledging the fact that some ‘buffer’ must be built into the BOL catalyst loading to account for inevitable losses/degradation to the anode catalyst layer. Two examples of important anode losses include ‘reversal’ events and contamination in the fuel stream. Reversal (or hydrogen starvation) events occur when the anode fuel is not able to access the anode catalyst layer. This can commonly occur during subzero events, during which time ice can form in the anode flow fields. As current is passed through the fuel cell stack, any MEA anode which does not have a supply of H₂ is driven to exceedingly high (>1.5 V) voltages. When this occurs, the anode catalyst is rapidly degraded, largely through severe carbon corrosion leading to loss of electronically connected Pt. The use of oxygen evolution reaction (OER) catalysts in the anode layer can help to mitigate this degradation [80], but some degree of anode degradation is highly probable. In terms of contamination, one of the most common methods for producing H₂ has been steam reforming and the water gas shift reaction. When H₂ is generated this way, there is invariably trace CO in the fuel which can poison the surface of the catalyst [81]. As the CO blocks the surface, the effective area of the catalyst is reduced, which is phenomenologically the same as a decrease in loading/Pt surface area. Thus, as Pt loadings at the anode are decreased, the sensitivity towards CO contamination is greatly increased (Fig. 3B). Though excellent work has been done in the past to deal with CO tolerance, including the development of PtMo CO-tolerant catalysts [81,82], anode electrocatalyst susceptibility under ultra-low Pt loading conditions is yet to be discerned, but it may be imperative to have ultra-pure H₂. With these points in mind, it is clear that even if a minimal performance impact is observed at an anode loading of 0.025 mg/cm², targeting such a loading with conventional anode catalysts would be exceedingly risky for a commercial product.

The mechanism for the loss in Fig. 3A is quite clear, and is easily explained through a linearization of conventional Butler-Volmer kinetics, assuming anode polarization is $< \frac{RT}{\alpha F}$ (~ 50 mV) (Eq (2)) [83].

$$\eta = \frac{i}{i_o} \frac{RT}{F(\alpha_a + \alpha_c)} \quad (2)$$

This is valid for the anode in a PEMFC, where the polarization is typically no more than ~ 10 mV. Eq. (2) highlights that the anode losses take the form of Ohm’s law ($V=IR$), with the resistance term equal to $\frac{RT}{i_o F(\alpha_a + \alpha_c)}$. With this knowledge, the data in Fig. 3A can be fit using Eq. (2) at various current densities, as shown in Fig. S1.

When looking at Eq. (2), it appears that the inherent kinetics of the HOR (either the exchange current density or transfer coefficient) will have to be improved in order to help mitigate this issue. While it should be noted that more advanced anode performance models exist (which include mass transport effects) [79], the simplicity of Eq. (2) combined with the reasonably good fit to experimental data suggests that kinetic

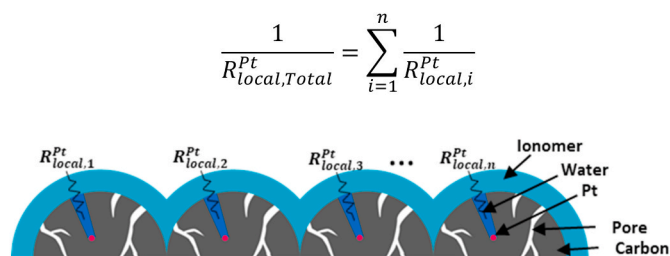


Fig. 4. Schematic showing how the local Pt resistance decreases with increasing number of active Pt sites. In this schematic, the Pt is assumed to be housed inside pores, but the same result is true for ‘external’ Pt.

limitations are likely the primary contributor at these ultra-low loadings.

Realistically, there is likely nothing that can be done to improve the transfer coefficient of the HOR, which is directly related to the rate-determining step in the reaction [83]. In the case of the HOR/HER, the mechanism is relatively elementary, with α_a and α_c both equal to 0.5 [84]. It is worth noting that some authors have reported HOR transfer coefficients >0.5 , but as highlighted in an excellent paper by Gasteiger et al. [84], this was largely due to a misuse and/or misunderstanding of RDE methods to evaluate HOR kinetics. Thus, at this juncture of PEMFC research, it may now become important to start actively investigating novel HOR catalysts with improved turnover frequency (i_o) vs. Pt, in much the same way novel ORR catalysts have been studied over the past several decades. The HOR exchange current density (i_o) for Pt/C can be extracted from the fitted data in Fig. S1, giving a value of ~ 220 mA/cm², which is close to those previously reported at the MEA level (20–100 mA/cm²) [85]. Fortunately, when examining the ‘volcano plot’ for the HOR, there does appear to be room for improvement, possibly through the development of new Pt alloys (Fig. S2). The expected impact of an improved HOR i_o on anode voltage losses is also shown in Fig. S1, where it is evident that a 2x increase in the HOR i_o would enable a 50% decrease in anode Pt loading for the same anode voltage losses, or provide some performance ‘buffer’ towards CO contamination.

2.3. Cathode performance losses at low PGM loadings

As is the case with many phenomena in PEMFC research, the situation at the cathode proves to be much more complex than at the anode. In MEA testing, at low current densities, any performance loss from decreased PGM loadings can be successfully offset by an equivalent increase in mass activity of the catalyst, as would be expected based on conventional electrochemistry. Unfortunately, it has now been well documented [15,86–89] that as current densities are increased to ≥ 1.5 A/cm², a large decrease in performance is observed for cathode PGM loadings $< \sim 0.1$ mg/cm². The source of this performance loss has been the focus of intense research over the past decade, and the importance of this work to the PEMFC industry is highlighted by the fact that the majority of the research in this area has been dominated by automotive OEMs, including Nissan [87], Toyota [90,91], and General Motors [86]. Furthermore, while catalyst durability falls outside the scope of the present review, it must be noted that any performance limitations observed at these low loadings will only be exacerbated by normal catalyst degradation mechanisms including both dissolution and carbon corrosion. While carbon corrosion can be largely mitigated through system level strategies, Pt dissolution is still a major concern, with conventional accelerated stress tests showing anywhere from 20 to 80% of the initial Pt area being lost depending on the upper potential limit used during the test [92]. For a more detailed discussion on current durability challenges, readers are directed to several recent catalyst-specific reviews [10,16].

Several studies have now clearly shown that this loss increases as the local flux of O₂ to each Pt site is increased, and it is thus often referred to

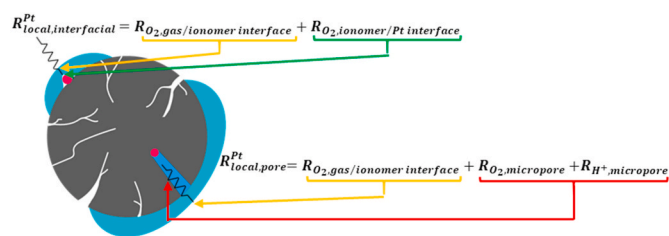


Fig. 5. Schematic showing the various contributions for both ‘external’ and ‘internal’ Pt. Note, the Pt housed inside the pore is depicted as being in contact with water (not ionomer) which is why $R_{O_2,ionomer/Pt interface}$ is assumed to be nil for this Pt particle.

as a ‘local O₂ transport loss’ (R_{local}^{Pt}) to help differentiate it from traditional transport losses (e.g. in the microporous layer). It is important to note that R_{local}^{Pt} is not dependent on overall catalyst layer thickness, but rather, on total available Pt area expressed in terms of MEA ‘roughness factor’ (R.F. = cm² Pt/cm² MEA) [88]. Conceptually then, it is most helpful to envision the total R_{local}^{Pt} as being the sum of many parallel resistors, such that R_{local}^{Pt} decreases as the number of resistors increases (Fig. 4).

R_{local}^{Pt} is relatively pressure independent, suggesting it is a non-fickian transport loss. In 2012 Greszler et al. [86] developed a thorough analysis of R_{local}^{Pt} , relating it to other non-Fickian losses through Eq. (3).

$$R_{NonFickian} = \frac{4FC_o}{i_{limiting}} = R_{MPL+CCL} + \frac{R_{O_2}}{R.F.} \quad (3)$$

It was shown that R_{local}^{Pt} can be directly measured through limiting current measurements at various oxygen concentrations. Through this analysis, the authors determined that R_{local}^{Pt} was ~ 12 s/cm for their particular catalyst. The authors demonstrate that if bulk ionomer properties are assumed, an oxygen transport resistance of 12 s/cm would imply the Pt catalyst is covered by ~ 35 nm thick ionomer films, or that the catalyst/ionomer agglomerates are ~ 380 nm in diameter. However, as the actual ionomer film thicknesses were ~ 4 –10 nm (assuming uniform distribution of ionomer), and the agglomerates observed using scanning electron microscopy (SEM) were far smaller than 380 nm, this large value of R_{local}^{Pt} was left as an important and intriguing mystery, likely related to the very unique physical properties of thin ionomer films [93].

Since this time, many groups have measured R_{local}^{Pt} , with values ranging from 10 to 40 s/cm. The relationship between these predicted R_{local}^{Pt} losses and roughness factor (R.F.) is give in Fig. S3. It is clear (Fig. S3) that lower R_{local}^{Pt} values will allow for lower R.F.s (and thus PGM loadings) to be achieved before significant transport limitations are experienced. For reference, in Fig. S3 the expected Pt loading at each R.F. is also shown on a secondary axis assuming a fairly typical Pt size of 5 nm. It is evident from this plot that even when taking the low end of reported R_{local}^{Pt} values (~ 10 s/cm), the total non-Fickian transport losses begin to greatly increase at Pt loadings of ≤ 0.1 mg/cm².

2.3.1. Mechanistic origins of R_{local}^{Pt}

Several possibilities for the mechanistic origins of R_{local}^{Pt} have been proposed, including: 1) anion interactions [86,94], 2) water management [95], and 3) a high interfacial resistance at the gas/ionomer and/or ionomer/Pt boundaries as a result of changes in the properties of thin ionomer films vs. bulk layers [86,88,90]. While mechanism 1 and 2 may very well contribute to the observed performance loss, currently mechanism 3 appears to have the most support from both a theory and experimental aspect and will therefore be the focus of this discussion. If this mechanism is correct, the question becomes whether the limiting transport step is at the gas/ionomer phase or the ionomer/Pt interface. This has large implications on how to design ideal carbon supports. If the

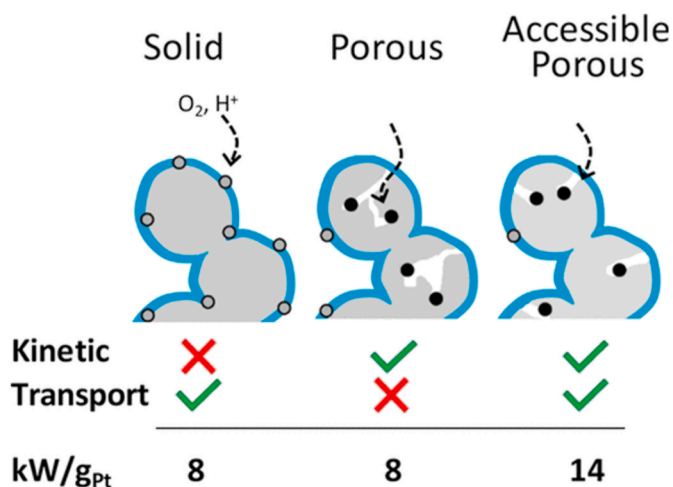


Fig. 6. Schematic showing the impact of carbon pore structure on kinetic and transport losses [4], reprinted with permission from the American Chemical Society.

ionomer/Pt phase is rate limiting, then preventing Pt from being in direct contact with the ionomer (deposit into pores too small for ionomer penetration to occur) could help to alleviate the problem, provided the Pt is still within close proximity to the ionomer to prevent additional transport losses (Fig. 5). Alternatively, if the gas/ionomer phase is most critical, a different strategy would be necessary, such as changing the physical structure/chemistry of the ionomer.

This question was studied by Toyota, with molecular dynamic modelling suggesting that the largest transport resistance is in fact at the ionomer/Pt interface [91] ($R_{O_2,ionomer/Pt\ interface}$ in Fig. 5), providing hope that properly tuned carbon structures could be used to overcome this challenge. Experimental evidence to support this conclusion was also provided by Liu et al. [94] through the use of a novel experimental arrangement which allowed the authors to separate out oxygen transport phenomena from electrochemical phenomena (i.e. potential dependent anion adsorption) by preventing the ionomer film from being in direct contact with the Pt surface. While the exact mechanism cannot be elucidated by this study, the authors did demonstrate that the gas/ionomer phase was not a major contributor to performance losses, seemingly in agreement with the modelling study [91]. Overall, these findings initially appear to suggest that housing Pt inside the pores of carbon structures may help reduce R_{local}^{Pt} by preventing direct contact with the ionomer to reduce $R_{O_2,ionomer/Pt\ interface}$, while also improving mass activity by preventing ionomer poisoning of the catalyst surface. However, it has been shown that when Pt is deposited inside porous carbon, the mass activity is improved vs. 'solid' carbon (as expected), but additional transport losses introduced by housing Pt in pores ($R_{O_2,micropore}$ and $R_{H^+,micropore}$ in Fig. 5) seem to overwhelm any benefits in the decreased value of $R_{O_2,ionomer/Pt\ interface}$ [4,96,97].

2.3.2. Effect of carbon support on R_{local}^{Pt}

The importance of transport losses within the pores of a carbon support was recently highlighted by General Motors [4]. In this work, the authors studied the R_{local}^{Pt} for three types of carbon structures (Fig. 6). The key differentiating point in this study vs. previous literature examining R_{local}^{Pt} was the prior knowledge regarding the spatial location of the Pt within the carbon structures.

As shown in Eq. (4), and noted by the authors in Ref. [4], R_{local}^{Pt} can be thought of as having contributions from interfacial resistance ($R_{O_2,interfacial}$) as well as transport resistance in the pores of the carbon ($R_{O_2,micropore}$). Based on the studies that have been performed to date, the interfacial and pore transport resistances can be further broken down into their believed origins (Eq. (4)):

$$R_{local}^{Pt} = \underbrace{R_{O_2,gas/ionomer\ interface} + R_{O_2,ionomer/Pt\ interface}}_{R_{local,interfacial}^{Pt}} + \underbrace{R_{O_2,micropore} + R_{H^+,micropore}}_{R_{local,pore}^{Pt}} \quad (4)$$

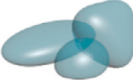
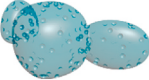
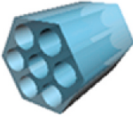
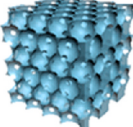
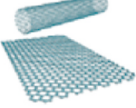
The $R_{O_2,micropore}$ and R_{H^+} ($R_{local,pore}^{Pt}$) terms in Eq. (4) are not new, as it has long been known that depositing Pt too deep into a carbon structure will introduce additional transport losses which may also result in poor performance at high current density [98,99], due to oxygen and/or proton transport as well as electrical resistance through the walls of the porous carbon material [100]. Rather, the interesting part of this study was to separate the relative importance of $R_{local,interfacial}^{Pt}$ vs. $R_{local,pore}^{Pt}$. For 'solid' carbon structures, whereby the Pt can be assumed to be deposited on the outer surface of the carbon and thus in direct contact with the ionomer, the R_{local}^{Pt} value was measured to be ~ 10 s/cm. When deposited in a 'porous' carbon, the R_{local}^{Pt} value increases to ~ 18 s/cm. Furthermore, for porous carbons having pore volumes ≥ 0.13 mL/g originating from mesopores in the range of 4–7 nm (considered to be more accessible by reactants but inaccessible to ionomer), the R_{local}^{Pt} value converges back to the same value as for solid carbons (~ 10 s/cm). The model put forward by the authors then for the 'accessible porous' carbons is of a structure whereby the Pt nanoparticles are not in direct contact with ionomer (thus $R_{O_2,ionomer/Pt\ interface}$ should be nil), but have wide enough pores such that $R_{local,pore}^{Pt}$ is minimized. However, if $R_{O_2,ionomer/Pt\ interface}$ was the largest contributor to $R_{local,interfacial}^{Pt}$ as was previously indicated [91,94], and was eliminated in the 'accessible porous' carbons, it is curious that the R_{local}^{Pt} value simply converged to the same value as for the solid carbons, where $R_{O_2,ionomer/Pt\ interface}$ should be quite prominent. This would seem to suggest that either $R_{local,pore}^{Pt}$ was not fully eliminated in the accessible porous carbons, and their remaining contributions nearly perfectly offset the elimination of $R_{O_2,ionomer/Pt\ interface}$ (a seemingly improbable scenario), or that $R_{O_2,gas/ionomer\ interface}$ actually dominates $R_{local,interfacial}^{Pt}$, which would contradict previous studies [91,94]. This result also highlights that our understanding of these losses is still at a relatively early stage, and it is likely that additional approaches (such as high oxygen permeable ionomers, optimization of water management in these ultrathin layers, and improving the distribution of ionomer within the catalyst layer) will also be required to fully maximize the performance. While it is clear that further work is required in understanding this phenomenon, these results do highlight the importance of developing new carbon structures, which will be critical in achieving the low Pt loading targets required for next generation PEMFC applications.

It is worth noting that in the early/mid 2000's, the development of novel/mesoporous carbon structures to act as Pt supports was being actively investigated [101–106], but the key role these structures may have in enabling ultralow Pt loadings was unknown by the research community at this time (including by the authors themselves). Practical MEA designs were still far from reaching Pt loadings of ≤ 0.125 mg/cm² Pt, and thus insufficient data/knowledge of $R_{local,interfacial}^{Pt}$ existed, and instead, the authors were focused on improving Pt dispersion as well as what would now be considered the $R_{local,pore}^{Pt}$ in Eq. (4). As current research efforts have begun focusing heavily on $R_{local,interfacial}^{Pt}$, the importance of $R_{local,pore}^{Pt}$ is now being rediscovered, and thus this earlier work is worth revisiting to help expedite the current research activities.

3. Development of carbon supports

The use of carbon to help support and disperse PGM catalysts was arguably one of the most significant technological advances in the PEMFC community [107], but in comparison to what has been achieved in advancing PGM catalyst research to the industry level, the carbon structure/design has remained relatively stagnant over the past several decades. This is not highly surprising, as until now, the required advances in PGM technology were so great that the need to focus on tuning

Table 3
Physical properties of various carbon supports for PEMFC applications.

Carbon Type	Surface area (m ² /g)	Pore size distribution	Carbon Particle size (nm)	Comments
 Vulcan carbon (VC)	220–240	Uncontrolled, but mostly < 2 nm	20–30	<ul style="list-style-type: none"> • Pt restricted to outer surface • Low mass activity but good high current density performance • Low corrosion resistance
 Ketjen Black	800–950	Uncontrolled, but contains both micro and mesopores	35–40	<ul style="list-style-type: none"> • Pt housed within pores • High mass activity but poor high current density performance • Low corrosion resistance
 OMCs	600–2800	3–40 nm	20–1000	<ul style="list-style-type: none"> • Very high surface area • Can achieve small Pt particle size at high Pt loading • Pt housed inside pores • High mass activity but poor high current density performance
 Inverse Opal	100–800	15–100 nm	100–1000	<ul style="list-style-type: none"> • Moderate surface area • Can control pore depth • Pt housed inside pores • Limited MEA data available
 Carbon Nano Tubes (CNTs)/Graphene	200–700 (CNTs) ~2600 (graphene)	1–20 nm (CNTs) N/A (graphene)	<10 μm	<ul style="list-style-type: none"> • High surface area • Corrosion resistant • Can be difficult to deposit Pt without surface functionalization

carbon structure was comparatively low. However, recent MEA integration activities are now highlighting the critical role that carbon structure can play in helping to achieve ultralow PGM loadings. The following provides a brief review of the main approaches that have been used to improve upon conventional carbon structures, and follows with a short discussion of what advanced carbon structures could be targeted. Some of the previously employed strategies are summarized in Table 3.

3.1. Commercial carbon

For the past two decades, the most common commercial carbon supports have been carbon blacks such as Vulcan carbon XC-72R, Ketjen Black, and to a lesser extent, Plack Pearls [108]. Carbon blacks are composed of relatively amorphous spherical carbon particles (typically 10–500 nm in diameter) which agglomerate into much larger particles of 100–800 nm. Their surface areas typically range from 100 to 1500 m²/g, and it is this high surface area that has made them such attractive options when attempting to disperse PGM catalysts. While they certainly cannot be considered ‘graphitic’, the conductivity of these materials have proven sufficient such that protonic resistance through the ionomer in the catalyst layer is often assumed to far outweigh any Ohmic losses through the carbon [109,110].

The primary limitation of these commercial carbons is their relatively uncontrolled porous structure, which in turn leads to a very limited ability to spatially distribute the PGM catalyst in an ideal manner. While electron imaging and/or electrochemical techniques have been able to verify that certain conventional PGM/C structures have more ‘inner’ or ‘outer’ PGM particles [4,111], these results are not necessarily by design, but rather an unintended consequence of the pore structure of the commercial carbon used to prepare the catalyst. Recently, it was reported that by tuning the experimental properties for

Pt deposition onto commercial carbon, the spatial distribution of Pt within the pores of a commercial carbon can be somewhat controlled [96], but without a controlled porous structure, design options are limited.

3.2. Modification of commercial carbon

The concept of modifying carbon surfaces is itself not new [108,112, 113]. One effective approach to achieve enhanced-performance is to introduce heteroatoms (e.g. Nitrogen) into carbon supports. Nitrogen functionalized carbon supports, such as VC, CNT and porous carbon, have shown great potential for realizing increased ORR activity, higher power density and improved long-term cycling durability by minimizing both carbon corrosion and Pt dissolution. Traditional carbon supports (at both the anode and cathode) can suffer from corrosion due to high potential excursions, moisture, and hydrogen peroxide [114]. Schmies et al. quantitatively investigated carbon corrosion by High-Temperature Differential Electrochemical Mass Spectroscopy (HT-DEMS) [115]. Compared to N-modified VC, unmodified VC displayed a sharper increase in corrosion current accompanied by a larger increase in mass ion current with $m/z = 44$ for CO₂ above 0.9 V (Fig. S4). This suggests that the high degree of N-surface functionalization is beneficial for carbon stability.

N-doping has also been found to have a positive impact on minimizing Pt dissolution. Nitrogen is more electronegative than carbon, and consequently electron density is transferred from the adjacent C atoms to the N dopant, allowing for stronger anchoring of Pt nanoparticles [114], as confirmed by DFT calculations [116]. XPS analysis has also shown that additional N doping leads to a slight shift of the Pt 4f peaks to higher binding energy, which could be ascribed to electron transfer from the deposited Pt nanoparticles to the N dopants, likely strengthening

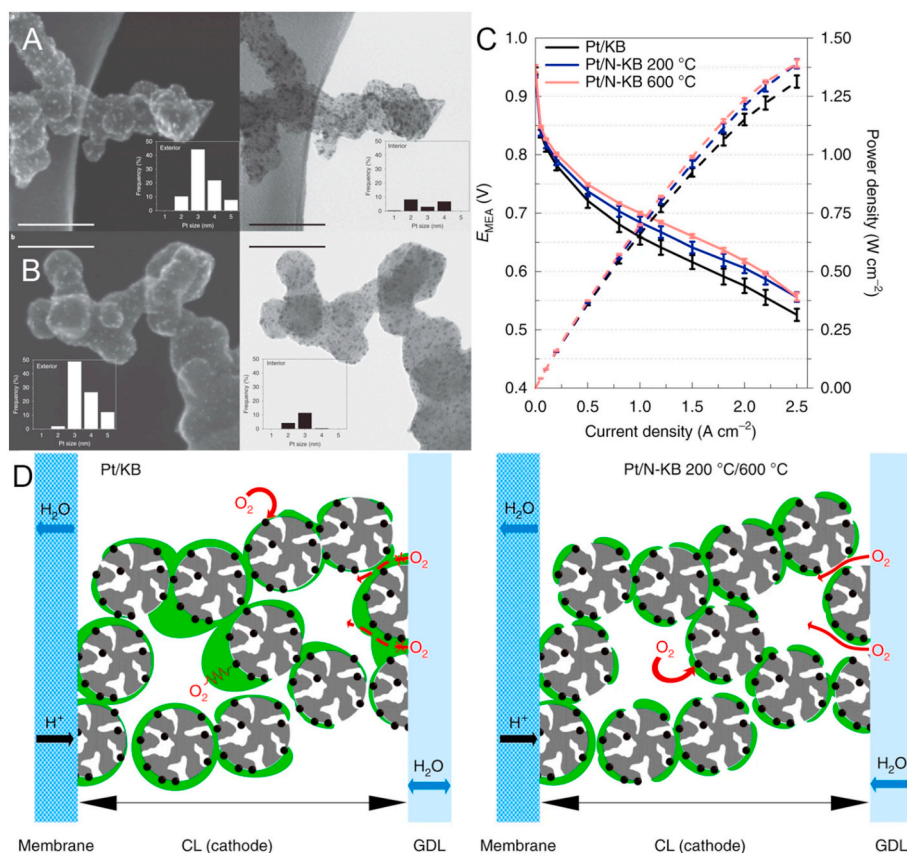


Fig. 7. (A) SEM and transmission SEM (TSEM) imaging of Pt/N-KB 600 °C and (B) Pt/KB following Pt loading through the polyol method. (C) MEA polarization curves of the two catalysts. (D) Schematic illustration of the Knudsen resistance for oxygen transport within the catalytic layer (CL) for badly distributes ionomer layers (left) and good ionomer distribution over the entire catalyst (right) [118], reprinted with permission from Springer Nature.

their interaction [116]. This enhanced interaction between Pt and the carbon support helps to eliminate the possibility of Pt nanoparticles aggregating into larger particles or dissolving into the polymer electrolyte, which preserves the Pt surface area thus leading to higher MEA durability.

While the potential durability benefits of such N-modified carbons are well studied, the critical importance of this approach on achieving ultralow PGM loadings is only recently becoming evident [96,117,118]. In recent work by Gasteiger et al. [117], the authors performed an ammonolysis treatment to conventional VC. They then loaded the functionalized carbon with Pt (Pt/V-NH_x), and compared the properties to a similarly loaded ‘as-received’ carbon (PtV-NH). VC is generally believed to be a ‘solid’ carbon, such that the Pt is confined to the outer surface. Thus, PGM catalysts deposited on these supports typically show low mass activity due to ionomer poisoning. The aim of this work was to improve the ionomer distribution on the surface of the catalyst through favorable interactions between the sulfonate group in the ionomer and the NH_x groups on the surface of the carbon. Both RDE and MEA testing revealed no difference in mass activity between Pt supported on VC vs. V-NH_x supports. Interestingly, in a subsequent publication the same authors perform a similar set of experiments but with Ketjen black instead of VC, and demonstrate that functionalized Ketjen black shows lower mass activity in an MEA vs. ‘as received’ Ketjen black, which they use as evidence for improved ionomer coverage [96]. This difference in observations for the VC vs. Ketjen study may be due to the large differences in surface area between VC (~240 m²/g) and Ketjen black (~900 m²/g), whereby ‘inhomogeneous’ ionomer coverage of VC still results in full coverage of the Pt particles such that nearly all of the Pt surface is already blocked by ionomer even for the unmodified VC. However, the inherently speculative nature of this discussion does

highlight the broader PEMFC community need for improved catalyst layer characterization methods to provide more definitive answers.

The high current density MEA data for Pt/V-NH_x was much improved vs. Pt/V, which is ultimately attributed to a more uniform ionomer coverage on Pt/V-NH_x leading to an optimal tradeoff between oxygen and proton transport in the layer. This result appears to have little to do with Eq. (4) and R_{local}^{Pt} , but rather, is related to the more traditional (and equally important) concept of gas transport in bulk ionomer in the catalyst layer. While the authors achieved their result through a materials-level modification, it is also possible to greatly impact the homogeneity of the ionomer in the catalyst layer through optimization of the catalyst ink solvent system/mixing methods, and thus highlights that catalyst layer-level strategies may also play a key role in overcoming remaining performance challenges.

Following on this work, the same authors combined the concept of carbon functionalization with synthetic approaches to control the spatial distribution of Pt within a carbon support [96]. For this study, the authors selected Ketjen Black, as the porous structure of Ketjen black allows for the deposition of both internal and external Pt particles (in contrast to the predominantly microporous nature of VC which ensures that the Pt is nearly completely confined to the surface of the carbon particles [102]). The spatial distribution of Pt was varied by tuning the concentration of the Pt precursor and reduction method (high concentration combined with polyol reduction lead to a higher percentage of surface particles) during the Pt loading experiments. Strong evidence for the spatial location of Pt within the carbon support is not provided, as only conventional TEM imaging was available, but the results do appear to at least provide some evidence that the authors were able to vary the percentage of inner vs. outer Pt particles through this approach. For the catalyst believed to possess Pt primarily on the outer surface of the

carbon (Pt/KB_{P0}), the observed ECSA measured in the MEA was lower than that obtained in ionomer-free RDE testing. This provides further evidence that Pt was primarily located on the outer surface, as ionomer contamination of a Pt surface has previously been shown to result in a decreased ECSA [45]. However, following this same line of reasoning, it is odd that the specific activity ($\mu\text{A}/\text{cm}^2$) of the catalyst assumed to have Pt mostly deposited on inner pores (Pt/KB_{IW}) was nearly identical to the catalyst assumed to have Pt mostly deposited on the outer surface (Pt/KB_{P0}), as the Pt on Pt/KB_{P0} should have had more direct contact with ionomer leading to a lower specific activity [45]. In fact, the expected decrease in specific activity would be even larger than the decrease in ECSA due to an increased coverage of sulfonate anions at ORR relevant potentials (vs. much lower potentials during ECSA measurements) [119].

Regardless, measurements of the pressure independent oxygen transport resistance reveal higher values for the catalysts which contain Pt within their inner pores, thus speaking to the importance of $R_{local,pore}^{Pt}$ in Eq. (4). These results would also be in agreement with those published by GM [4], where it appears any benefit of eliminating $R_{O_2,ionomer/Pt\ interface}$ is overwhelmed by the large contribution of $R_{local,pore}^{Pt}$ in Eq. (4).

Building on these studies, recent work by Strasser et al. [118] used a similar ammonolysis of Ketjen Black, but in addition to repeating the work at 200 °C, also performed experiments at higher temperatures of 400 or 600 °C to both functionalize the carbon surface as well as modify the porous structure to more ideally house the Pt particles. At 400 or 600 °C, the carbon structure was etched in a similar fashion to that utilized by the NPMC community [61] leading to an increase in pore diameter and higher percentage of mesopores. The polyol reduction method previously described was then used in an effort to restrict the deposited Pt particles primarily to the outer surface of the porous carbon (Fig. 7). The measured mass activity for the sample processed at 600 °C (Pt/N-KB 600) was found to be >50% higher vs. that at 200 °C (Pt/N-KB 200), suggesting that fewer of the Pt nanoparticles in Pt/N-KB 600 are in direct contact with ionomer vs. Pt/N-KB 200 where a higher degree of anion poisoning from the ionomer can occur. Importantly however, transmission scanning electron microscopy (TSEM) data demonstrated that the Pt in the Pt/N-KB 600 sample was still primarily located near the outer surface of the particle, which when combined with the mass activity data, suggests these Pt particles are being housed in the openings of the mesopores very near to the carbon surface. Such a structure appears to be closer to an ideal spatial distribution, whereby the Pt can avoid direct contact with ionomer to minimize $R_{O_2,ionomer/Pt\ interface}$ but is still in close proximity so $R_{local,pore}^{Pt}$ in Eq. (4) is minimized.

When examining the polarization data under air, the N-modified Ketjen Blacks do show performance benefits compared to the unmodified Ketjen Black (Fig. 7C), which the authors attribute to an improved ionomer distribution (Fig. 7D) as previously described by Gasteiger et al. [117]. Pt/N-KB 600 °C shows the highest performance until current densities of >2 A/cm², and the ~20 mV higher performance of this catalyst vs. Pt/N-KB 200 °C is in good agreement with the ~50% higher mass activity of Pt/N-KB 600 °C vs. Pt/N-KB 200 °C. However, at > 2 A/cm², the performance of Pt/N-KB 600 °C begins to decrease dramatically, which suggests transport limitations to Pt sites inside the catalyst. As with the previous studies, this result again indicates that the $R_{local,pore}$ term may overwhelm any benefit from reducing $R_{O_2,ionomer/Pt\ interface}$ in Eq. (4).

Finally, the stability of these functional groups was evaluated following a standard voltage cycling analysis. All catalysts (including the unmodified Pt/KB) show ~ 40% loss in ECSA following the cycling experiment. Perplexingly, only Pt/KB shows the expected low current density voltage loss of ~15 mV that would be inherent following a 40% decrease in ECSA (again, assuming standard Butler Volmer kinetics), whereas the modified catalysts show essentially no change in low current density performance despite also experiencing a 40% decrease in

ECSA. The authors again attribute this odd result to a uniform coverage of ionomer, but it is unclear how this explanation accounts for the observation.

3.3. Ordered mesoporous carbons (OMCs)

3.3.1. Background and motivation

OMCs are prepared through the use of a hard-template or soft-template approach. The hard-template strategy generally employs an ordered mesoporous silica (OMS) framework that is later etched out through the use of NaOH or HF [103,120,121]. The resultant OMC is thus an inverse reflection of the dimensions of the OMS. In the soft-template method, soft templates (e.g., Pluronic block copolymers) and precursors are self-assembled into ordered mesostructures [122–124]. Carbonization in inert atmosphere results in OMCs with similar mesostructures as templated liquid crystals [125,126]. OMCs typically have very high surface areas (600–2800 m²/g [120,127]), thus allowing for excellent distribution of Pt nanoparticles which has caused them to attract significant attention as potential Pt supports for ORR catalysts [99,103–106,128,129].

3.3.2. Experimental studies

In 2001, Joo et al. [103] reported the first ORR data for a Pt/OMC catalyst based on the use of a Santa Barbara Amorphous (SBA-15) template. This OMC possessed hollow tubes having a pore diameter of 5.9 nm and a spacing of 4.2 nm between pores. This OMC reportedly had a surface area of 2000 m²/g, which enabled deposition of 2.5 nm Pt nanoparticles at as high as 50 wt% Pt loadings. In contrast, the authors suggest that at similar wt.% Pt loadings on conventional carbon blacks, the Pt size was closer to 30 nm. It should be noted that this is certainly not universally observed, with many commercial catalysts achieving 2–3 nm Pt particle sizes on carbon black supports. The authors did report a much higher mass activity for their catalyst vs. a more conventional Pt/C. However, in this early work, the benefit was primarily attributed to the smaller Pt particle size achieved in the OMC support vs. a conventional carbon black as opposed to preventing direct contact with ionomer.

The promise of this work spurred further research on the development of Pt/OMCs catalysts. However, as research advanced beyond RDE testing, the early MEA testing results clearly indicated that, as would now be expected, these structures result in improved mass activity but suffer from poor performance at high current densities [99,104,129] likely as a result of reactant transport limitations to the Pt nanoparticles deposited within the pores of these carbons. This appears to be exactly what is now being observed by the fuel cell community for more conventional carbons, as researchers begin to study tradeoffs between Pt spatial distribution and MEA performance.

For templated carbons such as these, there is an additional consideration related to the electronic conductivity of the carbon walls. While electronic conductivity is always an important factor, the importance is amplified for OMCs due to their extremely high porosity, such that the available carbon pathways are limited. The question of whether wall thickness or inherent resistivity is easier to tune was investigated by Birss et al. [100]. The authors used a single OMS template to prepare three different OMCs, using either sucrose, naphthalene, or anthracene as a carbon precursor. It is known that to form graphite crystallites, the more energetically difficult stage is building of the sp² hybridized aromatic rings, as opposed to the pi-pi stacking of these aromatic graphene planes [108]. Thus, by varying the precursor from sucrose (no aromatic rings) to naphthalene (two aromatic rings) to anthracene (three aromatic rings), the final graphite crystallite size (and thus wall conductivity) was varied while maintaining the same wall thickness. In addition, the authors then prepared three OMCs using one carbon precursor, but using three different OMS templates, resulting in a second series of OMCs having the same degree of carbon crystallinity, but different wall thicknesses. These OMCs were all loaded with Pt, followed

by RDE testing. The results suggested that, at least through the synthetic approach used by the authors, wall thickness was easier to tune than inherent conductivity.

3.3.3. Challenges for OMCs

Unfortunately, it is highly challenging to prepare silica templates with ever increasing wall thicknesses, and thus the pore diameter of OMCs is typically limited to <7 nm [130]. Structurally then, these carbons are more similar to Ketjen black than VC, as their pore diameter is large enough to house Pt in the interior of the particle. While the ability to tune pore diameter is certainly an improvement on Ketjen Black, it may be expected that the performance of OMCs as a Pt support will suffer from the same problems as Ketjen Black (e.g., high mass activity due to ionomer not being in direct contact with the Pt, but a large contribution from $R_{local,pore}^{Pt}$ leading to poor performance at high current densities).

3.4. Inverse opal carbons

3.4.1. Background and motivation

Another class of hard templated carbons rely on the self-assembly of nanoparticles, most typically SiO₂. The SiO₂ nanoparticles assemble into a close packed hexagonal structure, creating a synthetic opal. The spacing between the individual SiO₂ nanoparticles can then be infiltrated with a carbon precursor, such as phenol and formaldehyde [131] followed by carbonization. The SiO₂ framework is then etched out using NaOH or HF, leaving an ‘inverse opal’ structure [132–135]. These carbons offer some benefits over OMCs, in that the pore diameter is more easily tuned by simply varying the size of the SiO₂ nanoparticles used in the synthesis. There are variations on this theme, including the use of larger polystyrene beads in combination with SiO₂ nanoparticles to prepare carbons having multi-scale pore structures [136].

Perhaps the most promising of this class of carbons are the colloid imprinted carbons (CICs) originally reported by Jaroniec et al. [130]. In their work, the authors use a unique synthetic strategy that relies on the use of a carbon-based mesophase pitch which is ‘imprinted’ into the synthetic opal structure. The viscosity of this pitch can be controlled by varying the temperature used during the imprinting phase. The key advantage of this approach is that it allows for control not only over pore diameter, but pore depth as well. Additionally, the synthetic naphthalene-based mesophase pitch used in this work consists of large sp² hybridized molecules, making the final carbon structure highly graphitic and thus highly conductive. The ability to tune pore depth represents a potentially more reliable way of tuning ‘inner’ vs. ‘outer’ Pt [4,96], as the core of the shallow imprinted carbons is mostly nonporous. Through tuning both pore diameter and depth together, it should also be possible to identify the most optimal tradeoff among all terms in Eq. (4).

3.4.2. Experimental studies

The first use of CICs as a support material for Pt ORR catalysts was reported by Fang et al. [137]. The authors prepared a CIC having 22 nm pores, and loaded it with 20 wt % Pt. Significantly, the MEA results of this catalyst did not demonstrate the same degree of mass transport limitations as those observed for OMCs, suggesting the larger pore diameter of these CICs helps to minimize transport losses ($R_{local,pore}^{Pt}$ in Eq. (4)) within the pores. Unfortunately, it is not clear from this work whether the ionomer was also able to penetrate into the pores and poison the Pt surface.

Following on this work, a series of CIC studies were performed by Birss et al. [101,102,128,138]. The most relevant of these studies to the current review was work focusing on the effect of carbon pore depth, representing the first time such a study had been performed [101]. In this work, 22 nm SiO₂ colloids were used to prepare CICs all having pores of 26 nm (slight enlargement vs. the SiO₂ colloids was observed),

but each with a different pore depth which was controlled by varying the imprinting temperature from 250 °C–400 °C). These supports were loaded with 20 wt% Pt, and fully characterized using conventional physical characterization methods. The surface area of the CICs was found to increase with increasing imprinting temperature, and the Pt nanoparticles deposited on the lower surface area carbons (lower imprinting temperature) were larger (~6 nm) vs. those on the higher surface area CICs (~3.5 nm) as may be expected based on total number of nucleation sites available on low vs. high surface area supports. In addition, 3DTEM/TEM tomography was used to verify the structure of these carbons, as well as the spatial location of Pt. It was confirmed that the average pore depth had been varied for this series of carbons, and that Pt had been successfully loaded throughout the entire porous structure, allowing for a reliable study on the impact of carbon pore length. The RDE testing demonstrated no difference in inherent activity of these catalysts (once differences in ECSA due to differences in Pt particle size were accounted for), which indicated that at the RDE level no transport limitations were experienced. Unfortunately, the particle size of these CICs was too large (~1 μm) to perform reliable MEA studies, and thus it is still unclear whether these materials would show differences in performance in an MEA.

3.4.3. Challenges for inverse opal carbons

For these carbon structures, it is difficult to decrease the pore diameter to <20–30 nm in a controlled fashion, due to challenges in maintaining an ordered packing of SiO₂ colloids below this size as well as partial collapse of the porous carbon structure during carbonization due to the thin walls that result when infiltrating the spaces between such small SiO₂ particles [131,139]. For this reason, it may be difficult to prevent ionomer from penetrating into the pores, as the ionomer micelles typically range in size from 1 to 5 nm [140]. If ionomer does in fact penetrate into these pores, the MEA performance of this class of catalyst may be quite poor, as the ionomer could directly contact the Pt surface leading to anion poisoning, and both interfacial resistances ($R_{O_2,gas/ionomer\ interface} + R_{O_2,ionomer/Pt\ interface}$) in Eq. (4) would be present. While $R_{local,pore}^{Pt}$ in Eq. (4) would also be present, the larger pore diameter of inverse opal carbons means the magnitude of this term should be lower than for OMCs. It should be noted that although pores <20 nm are difficult to form while preserving an ordered structure in this class of carbon, it is still possible to form a ‘disordered’ porous network with pores having a diameter below this critical value [138]. As it is unclear how important the ordering will be on performance in an MEA, these carbons are certainly worthy of further investigation due to their unique pore structure and high degree of porosity control.

3.5. CNTs and graphene

3.5.1. Background and motivation

Both CNTs and graphene initially appear to be excellent candidates as carbon supports, as they possess high surface areas (Table 3). Additionally, the high degree of sp² hybridization of these materials provides them with a much higher electronic conductivity than carbon black [108], as well as improved corrosion resistance vs. VC [9,17]. However, pristine CNTs/graphite also pose a challenge when attempting to load them with Pt nanoparticles, as the paucity of defects/surface functional groups provides these materials with few nucleation sites for the Pt crystals to grow, and few anchoring sites to help prevent agglomeration. Thus, it is common for these carbons to be surface functionalized (often through treatment in HNO₃/H₂SO₄) prior to being loaded with Pt [141–144]. While many of these doped structures have been shown to possess inherent ORR activity (prior to the addition of PGM catalysts) [145–147], the activity of these doped carbons remains far from being relevant for the PEMFC industry, and thus presently, the primary commercial interest would be in their use as PGM catalyst supports. In addition to providing nucleation sites, the doping of CNTs/graphene

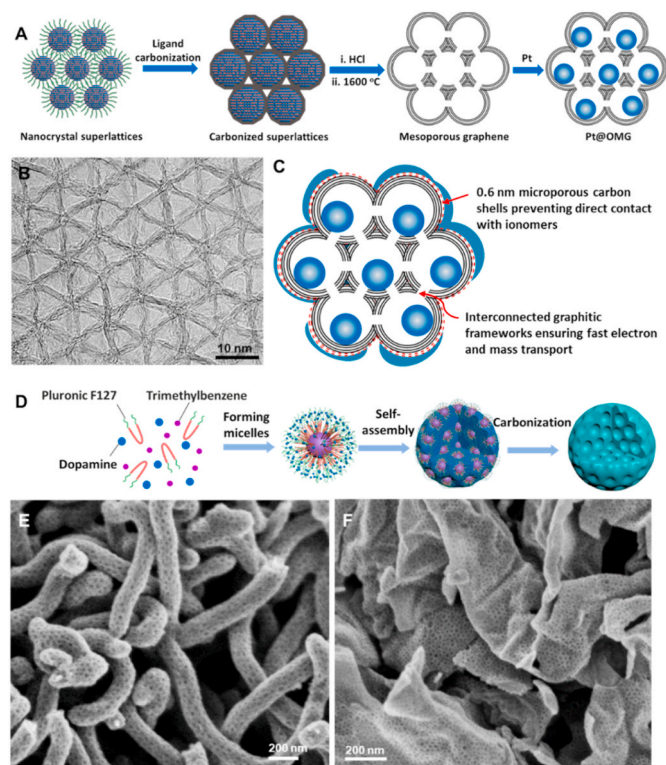


Fig. 8. (A) Schematic showing synthesis of OMG. (B) TEM image of OMG. (C) Schematic showing the structural merits of meso-microporous hierarchical graphene when used as the carbon support. (D) Schematic showing the synthesis of OMCs by self-assembly of monomicelles. (E) SEM image of OMC@CNTs. (F) SEM image of OMC@graphene.

with heteroatoms has been shown to lead to improve catalyst support interactions resulting in improved activity and durability [144,148].

3.5.2. Experimental studies

To help improve Pt dispersion, and interactions with the graphene support, Tiwari et al. [149] developed a novel approach based on the use of genomic double-stranded DNA-graphene oxide (Pt/gDNA-GO) support. While the specific advantages of gDNA vs. other chelating agents was not provided, the primary motivation was to use the strong interactions between the Pt^{2+} precursor and gDNA to help increase nucleation sites and anchor the Pt on the graphene. The Pt/gDNA-GO was reported to have a Pt particle size of ~ 0.8 – 1.4 nm vs. ~ 3 nm for the similarly loaded graphene oxide and a commercial Pt/C catalyst. As was previously discussed in this review, Pt particles $< \sim 2$ nm would in fact be expected to show low mass activity [23,24], and thus targeting such small particle sizes for the Pt/gDNA-GO would seemingly be ill-advised. However, the authors demonstrate much improved activity and durability for their Pt/gDNA-GO catalyst, which suggests that trends in activity/durability for Pt dispersed on traditional carbon supports may not be applicable to these novel materials. Chen et al. were the first to evaluate S-doped graphene as possible Pt supports for PEMFC applications. This work builds on the known strong interactions between Pt and sulfur. Whereas this strong binding has traditionally been a disadvantage (i.e. ionomer poisoning), the authors used this strong binding energy to their advantage, with the Pt/S-doped graphene catalyst showing greatly improved durability vs. similarly loaded Pt/graphene and a commercial Pt/C catalyst.

3.5.3. Challenges for CNTs and graphene

CNTs appear to have promise in helping to overcome the challenges associated with R_{local}^{Pt} as their pore diameters are tunable in roughly the

ideal range to both accommodate Pt while simultaneously excluding direct contact with ionomer. With these carbons, the primary challenges would likely be in developing synthetic approaches to ensure the Pt is deposited within the pores of the CNT (as opposed to externally), and in ensuring the CNT length is short enough that severe transport problems do not exist. Typically, CNTs are 1 – 10 μm in length, which would almost certainly result in poor MEA performance if Pt were to be housed inside due to an enormous increase in $R_{local,pore}^{Pt}$ in Eq. (4). It has previously been proposed that facile transport of protons through water can occur to Pt particles not in direct contact with ionomer provided that they are within ≤ 50 nm of the ionomer agglomerate [150]. Thus, if the CNT length could be controlled to $< \sim 100$ nm, Pt deposited within these pores could represent a promising direction for overcoming R_{local}^{Pt} . For graphene, the inherently non porous nature of the material makes it difficult to envision how this structure could be used to overcome R_{local}^{Pt} . It is most probable that PGM/graphene catalysts would show poor mass activity, and a high $R_{O_2,ionomer/Pt\ interface}$ much like other ‘nonporous’ supports (e.g. VC). Thus, graphene may not be an ideal candidate to serve as a PGM support for PEMFC catalysts moving forward.

3.6. Hierarchical mesoporous graphene

As mentioned above, despite its high electrical conductivity and superior chemical stability vs. carbon black, 2D graphene is not an ideal catalyst support for PEMFCs due largely to its non-porous nature. However, this issue could be addressed by designing a 3D mesoporous framework comprised of graphene. Such a structure, combining the benefits of both OMCs and graphene, represents a highly appealing option provided that the porosity of the material can be rationally tailored. In 2015, Dong et al. reported that colloidal nanocrystals of transition metal oxides such as Fe_3O_4 can be used to produce such an ordered mesoporous graphene (OMG) [151]. Specifically, Fe_3O_4 nanocrystals capped with organic ligands like oleic acid can be used as building blocks to construct superlattices by self-assembly (Fig. 8A). The subsequent pyrolysis of oleic acid ligands followed by acid etching of Fe_3O_4 nanocrystals yields interconnected mesoporous carbon frameworks inheriting the long-range ordered superlattice structure. Of course, the use of an Fe precursor raises some concerns in developing fuel cell materials, as Fe is a known Fenton’s catalyst and can lead to rapid degradation of the membrane [152]. Fortunately, a similar structure can be achieved using other transition metal oxides such as MnO.

OMG is obtainable by further heat treatment at temperatures over 1000 $^{\circ}C$, which converts the carbon frameworks into few-layer graphene (Fig. 8B). The resulting OMG is composed of interconnected spherical mesopores, possessing a surface area as high as 1000 m^2/g . The pore size of OMG can be readily tuned in the range of 5 – 20 nm by varying the size of Fe_3O_4 nanocrystals, while the windows between adjacent pores are about 2 – 3 nm. This range of pore diameter appears to be ideal for use as a PGM support in the PEMFC community. In principle, the Pt nanoparticles could be incorporated into the mesoporous graphene cores through an impregnation method. Importantly, the morphology of OMG can be tailored as spheres [153], films [154], and tubes [155], etc. by controlling the self-assembly behaviors of Fe_3O_4 nanocrystals. Among them, meso-microporous graphitic spheres, having mesoporous graphene cores and microporous carbon shells have been prepared [156]. This hierarchical graphitic structure is realized based on the transformation of Fe_3O_4 nanocrystal superparticles; the diameter of Fe_3O_4 superparticles and therefore meso-microporous graphitic spheres can be tuned in a range from 0.1 to 5 μm . The uniform microporous carbon shell, derived from a polypyrrole coating layer, has a tunable thickness ranging from a few to several tens of nanometers. Although this hybrid graphitic structure was designed for Li-S battery applications, this unique porous core/microporous shell structure offers intriguing potential both in terms of its highly graphitic nature, which is beneficial for

Table 4
Comparison of RDE and MEA test results among a variety of different Pt loaded carbons supports in literatures.

Carbon type	Features	Electrolyte	$E_{1/2}/V$	$J_{mass} 0.9 V/A mg_{Pt}^{-1}$	Cathode loadings/ $mg_{Pt} cm^{-2}$	Mass activity @0.9 V/A mg_{Pt}^{-1}	Difference in mass activity (RDE:MEA)	Power density/ $mW cm^{-2}$	Temperature/ $^{\circ}C$	Condition	Pressure	RH	Ref
CNTs				N/A	0.15	N/A	N/A	337.45 @0.65 V	80	H ₂ /O ₂	100 kPa	100%	[150]
CNTs	entangled			N/A	0.1	N/A	N/A	401.2 @0.65 V	80	H ₂ /O ₂	100 kPa	100%	[151]
CNTs				N/A	0.1	N/A	N/A	254.2 @0.65 V	80	H ₂ /O ₂	100 kPa	100%	[151]
CNTs	Pt-Ni; N-doped	0.1 M HClO ₄	0.887	0.02	0.12	0.177	-785.00%		80	H ₂ /air	150 kPa	100%	[152]
CNTs	free-standing			N/A	0.142	N/A	N/A	397.23 @0.65 V	80	H ₂ /O ₂	100 kPa	100%	[153]
CNTs	multiwall	0.1 M HClO ₄	0.85	0.48		N/A	N/A						[154]
graphene				N/A	0.2	N/A	N/A	161 @0.4 V	60	H ₂ /O ₂	atmospheric pressure	100%	[154]
graphene				N/A	0.5	0.024	N/A	124 @0.3 V	50–55	H ₂ /O ₂	atmospheric pressure	100%	[155]
graphene		0.1 M HClO ₄	0.73	N/A		N/A	N/A						[156]
graphene		0.1 M KOH	0.81	N/A		N/A	N/A						[157]
graphene		0.5 M HClO ₄	0.89	0.118 @0.85 V		N/A	N/A						[158]
KB	TEC10V20E	0.1 M HClO ₄	0.851	0.211	0.12	0.234	-10.90%	341.88 @0.7 V	80	H ₂ /air	150 kPa	100%	[152]
KB	TEC10EA20E	0.1 M HClO ₄	0.848	0.193		N/A	N/A						[153]
KB	TKK	0.1 M HClO ₄	0.84	0.33		N/A	N/A						[154]
KB	No ionomer	0.1 M HClO ₄		0.38	0.11	0.235	38.16%		80	H ₂ /O ₂	230 kPa	100%	[108]
KB	N doped; no ionomer	0.1 M HClO ₄		0.35	0.11	0.424	-21.14%		80	H ₂ /O ₂	230 kPa	100%	[108]
KB	TEC10E20E; no ionomer	0.1 M HClO ₄		0.982	0.062	0.372	62.12%		80	H ₂ /O ₂	170 kPa	100%	[86]
KB	no modification; no ionomer	0.1 M HClO ₄		0.336	0.064	0.249	25.89%		80	H ₂ /O ₂	170 kPa	100%	[86]
KB	Ketjen EC300J			N/A	0.056	0.38	N/A		80	H ₂ /air	150 kPa	100%	[4]
KB	Pt/Pd/C core-shell	0.1 M HClO ₄		0.95	0.1	0.4	57.89%		80	H ₂ /O ₂	140 kPa	100%	[14]
high-surface-area carbon	Pt-Ni alloy; sulfuric acid treatment			N/A	0.1	0.65	N/A		80	H ₂ /O ₂	150 kPa	100%	[8]
mesoporous	PyPBI coating carbon			N/A	0.45	N/A	N/A	342 @0.25 V	120	H ₂ /air	atmospheric pressure	dry	[159]
mesoporous	N doped			N/A	0.5	N/A	N/A	265.8 @0.6 V	70	H ₂ /air	atmospheric pressure	95%	[160]
mesoporous	N doped			N/A	0.5	N/A	N/A	474 @0.6 V	70	H ₂ /O ₂	atmospheric pressure	95%	[160]
nanofiber	carbon shell	0.1 M HClO ₄	0.889	0.075	0.1	N/A	N/A	500.4 @0.6 V	80	H ₂ /air	150 sccm of H ₂ and 800 sccm of air	100%	[161]
nanofiber	carbon shell; 30 k AST cycles	0.1 M HClO ₄	0.909	0.117	0.1	N/A	N/A	511.8 @0.6 V	80	H ₂ /air	150 sccm of H ₂ and 800 sccm of air	100%	[161]
OMC		0.5 M H ₂ SO ₄	0.83	0.212 @0.85 V		N/A	N/A						[162]

(continued on next page)

Table 4 (continued)

Carbon type	Features	Electrolyte	$E_{1/2}/V$	$J_{mass} 0.9 V/A mg_{Pt}^{-1}$	Cathode loadings/ $mg_{Pt} cm^{-2}$	Mass activity @0.9 V/A mg_{Pt}^{-1}	Difference in mass activity (RDE:MEA)	Power density/ $mW cm^{-2}$	Temperature/ $^{\circ}C$	Condition	Pressure	RH	Ref
OMC	SBA-15	0.5 M H_2SO_4	0.68	N/A		N/A	N/A						[163]
OMC	CMK-3	0.5 M H_2SO_4	0.66	N/A		N/A	N/A						[164]
OMC		0.1 M $HClO_4$	0.91	0.167		N/A	N/A						[165]
opal	Ordered macroporous			N/A	0.12	N/A	N/A	264 @0.6 V	80	H_2/O_2	cathodic dead-end mode	100%	[166]
opal porous	Ordered macroporous 3D porous graphitic	0.1 M $HClO_4$	0.878	0.301	0.12	N/A	N/A	633.6 @0.6 V	80	H_2/air	150 kPa	100%	[166]
porous	Pt-Co alloy; Co-N sites; ZIF-67	0.1 M $HClO_4$	0.941	8.64	0.033	1.08	87.50%		80	H_2/O_2	100 kPa	100%	[13]
porous	Pt-Co alloy; Co-N sites; ZIF-67			N/A		N/A	N/A	720 @0.6 V	80	H_2/air	150 kPa	100%	[13]
porous	Pt-Co alloy; Co-N sites; ZIF-8@ZIF-67			N/A		N/A	N/A	780 @0.6 V	80	H_2/air	150 kPa	100%	[13]
porous	Pt-Co alloy; Co-N sites; M ZIF-8@ZIF-67	0.1 M $HClO_4$	0.959	12.36	0.035	1.77	85.68%		80	H_2/O_2	100 kPa	100%	[13]
porous	Pt_3Co ; ZIF ₈	0.1 M $HClO_4$	0.837	0.91	0.043	0.417	54.18%		80	H_2/O_2	100 kPa	100%	[13]
VC	comercial			N/A	0.15	N/A	N/A	201.2 @0.65 V	80	H_2/O_2	100 kPa	100%	[150]
VC		0.1 M $HClO_4$		0.2		N/A	N/A			H_2/O_2			[167]
VC	comercial			N/A	0.1	N/A	N/A	210.7 @0.65 V	80	H_2/O_2	100 kPa	100%	[151]
VC	comercial; JM			N/A	0.5	0.028	N/A	27 @0.4 V	50–55	H_2/O_2	atmospheric pressure	100%	[155]
VC	comercial; JM			N/A	0.12	N/A	N/A	141 @0.6 V	80	H_2/O_2	cathodic dead-end mode	100%	[166]
VC	comercial; JM			N/A	0.12	N/A	N/A	621 @0.6 V	80	H_2/air	150 kPa	100%	[166]
VC	Vulcan XC72			N/A	0.062	0.11	N/A		80	H_2/air	150 kPa	100%	[4]

fast electron and mass transport, and in light of what is now known about ionomer/Pt interactions. In such a scenario, the pores of the mesoporous core could be expanded without concerns over ionomer penetration, as the thin (~several nm) shell with a pore size of ~0.6 nm would ensure the ionomer remained on the outer surface (Fig. 8C). Furthermore, by keeping the carbon particle size at a diameter of 0.1 μm , any PGM catalyst inside the structure would be at most 50 nm from the ionomer. Thus, this design may offer the best possible tradeoffs between all factors in R_{local}^{Pt} (Eq. (4)). A similar design can also be achieved through a molecule-mediated interfacial co-assembly strategy [157]. In this approach, block copolymers (e.g., Pluronic F127) assemble with carbon precursors (polymerized dopamine or resol) to form monomicelle-oligomers composites by molecule engineering (Fig. 8D). The monomicelle-oligomers composites act as the building blocks, which can assemble into mesoporous carbon materials or on the surface of graphene or CNTs to afford hierarchical OMC@CNTs (Fig. 8E) or OMC@graphene superstructures (Fig. 8F) [158,159]. While these structures have not yet been studied as possible fuel cell catalyst supports, the combination of OMCs with CNTs or graphene make these materials highly electronically conductive, and due to the flexibility afforded by this approach for tuning the thickness of the deposited OMC layers (monolayer to few-layer), as well as their pore diameter (2–40 nm), they appear to be a highly appealing option as both a model system, and possibly as a commercially viable carbon support.

RDE and MEA-level data for a variety of different Pt loaded carbon supports are summarized in Table 4. Due to the wide range of experimental methods used in the literature for RDE and MEA testing, it is not possible to draw firm conclusions regarding general trends in catalyst activity based on the carbon type. However, a few observations can be made.

First, while N-modification of commercial carbon enabled a mass activity of 0.424 A/mg for a Pt-only catalyst, no Pt-only catalyst has been able to achieve the targeted mass activity of ≥ 0.44 A/mg. This highlights the crucial needs for alloy catalysts in achieving ≥ 0.44 A/mg, but also suggests the combined approach of using alloy catalysts with the recent advances in carbon design may provide opportunities for previously unprecedented MEA-level mass activities.

Secondly, while it is somewhat rare to have both the RDE and MEA mass activities reported in the same study, there is sufficient data in Table 4 that some basic statistical analysis can be performed. It is known that, for the same catalyst, performing RDE studies without ionomer will lead to higher mass activities vs. RDE testing with ionomer [160]. As MEA catalyst layers do contain ionomer, it may initially seem likely that mass activities obtained through 'ionomer-free' RDE testing will show a larger discrepancy vs. RDE testing which uses ionomer when compared to MEA testing. To test this hypothesis, for each row in Table 4 where both RDE and MEA mass activities are available, the percent difference between the RDE and MEA reported mass activities was calculated. ANOVA was then performed to compare the group of data for which ionomer was used in the RDE testing vs. 'ionomer free' RDE testing. This analysis shows that within a 95% confidence level, the use of ionomer in the RDE testing resulted in no better predictive capability than ionomer-free measurements. Furthermore, when evaluating the data in Table 4, a strong correlation between the RDE and MEA measured activities is evident (Fig. S5A). While the linearity of this fit may appear to be strongly influenced by the two highest mass activities (resulting from the 'hybrid' class of catalysts, see Table 2), even when these points are removed a strong correlation is observed (Fig. S5B). This is contradictory to what some have previously reported [74] for RDE/MEA mass activities, but does support the claims of other authors that well performed RDE experiments can provide predictive trends at the MEA level [11,161,162]. While the data in Fig. S5 is not extensive, the fact that it does come from 6 independent publications provides some hope that RDE screening may not be as poor at predicting MEA activities as is often stated.

4. Conclusions and future outlook

Significant progress has been made at the materials-level in the development of high activity catalysts for PEMFC applications. However, as these materials have been integrated into MEAs, performance challenges at both the anode and cathode have become evident. At the anode, a kinetic limitation appears to have been reached, such that the development of new catalysts with higher activity vs. Pt towards the HOR may now be required. At the cathode, it has become clear that a transport phenomenon is limiting high current density performance for traditional PGM/C ORR catalysts, but the exact mechanism(s) behind this loss is (are) still not fully understood. While studies continue on developing a more complete understanding for cathode performance losses at low PGM loadings, it has become clear that catalyst support porosity will play a critical role in overcoming this challenge. Specifically, it is evident that key issues such as ionomer poisoning of the catalyst surface, ionomer/catalyst interfacial resistance, and reactant transport are all greatly impacted by the nanostructure of the carbon support.

Over the past decade, a number of studies have reported advantages of replacing traditional carbon black with novel porous carbons, including ordered mesoporous carbon (OMCs), inverse opal carbon, and CNTs/graphene. While each of these materials has its own unique advantages, none of them appear to have an ideal structure when reflecting upon what is now known about catalyst/ionomer interactions and achieving high current densities in MEA testing. The design of an 'ideal' pore structure may not yet be fully understood for carbon supports used in PEMFC applications, but the importance of porosity is now undeniable, particularly for low PGM loaded designs. When considering what is now known about R_{local}^{Pt} , and when examining previous studies on commercial as well as templated carbon materials, some speculation on ideal carbon structure is possible. It is now clear that housing Pt within a pore that is too small for ionomer penetration can have a large benefit in terms of mass activity, as it eliminates anion poisoning of the catalyst surface. Revisiting Eq. (4), it is also clear that Pt within such a pore should not experience any contribution from $R_{O_2,ionomer/Pt\ interface}$. However, this structure would show increased $R_{local,pore}^{Pt}$ vs. Pt deposited on the exterior of a carbon support. Therefore, it seems likely that the ideal carbon structure should possess a structure that can position the Pt as close as possible to ionomer, without having any direct contact. Alternatively, a balanced approach of having some Pt particles inside pores with other Pt particles located on the outer surface may show similar results. Through pursuing such options, MEA level mass activities for Pt-only catalysts have reached >0.4 A/mg, giving great hope that combining the advances in carbon structure with the latest generation Pt-alloy catalysts may enable previously unachievable MEA-level activities.

Ultimately, while it is evident that further research and materials development is required for both anode and cathode catalysts, there does appear to be pursuable options, which should ultimately unlock the possibility of commercializing MEAs with PGM loadings of <0.125 mg/cm². To fully achieve this goal, it is likely that these approaches will have to be combined with further strategies such as the use of high oxygen permeable ionomers, methods to improve ionomer distribution in the catalyst layer, design approaches to achieve durable/high ECSA catalysts, and new water management strategies within both the catalyst layers and microporous layers of the gas diffusion layer.

Declaration of competing interest

The authors declare that they have no known competing financial interests or personal relationships that could have appeared to influence the work reported in this paper.

Acknowledgments

The authors gratefully acknowledge funding from the Innovation Team of Universities of Guangdong Province (2020KCXTD011) and Guangdong Key Laboratory for Hydrogen Energy Technologies (2018B030322005), as well as from National Natural Science Foundation of China (22025501, 21872038, 21733003, 51773042, 51973040) and National Key R&D Program of China (2020YFB1505803, 2017YFA0207303).

Appendix A. Supplementary data

Supplementary data to this article can be found online at <https://doi.org/10.1016/j.jpowsour.2021.229515>.

References

- [1] Z.P. Cano, et al., Batteries and fuel cells for emerging electric vehicle markets, *Nature Energy* 3 (4) (2018) 279–289.
- [2] Global Automotive Executive Survey, 2017. KPMG.
- [3] J. Tollefson, Fuel of the future? *Nature News* 464 (2010) 1262–1264.
- [4] V. Yarlalagadda, et al., Boosting fuel cell performance with accessible carbon mesopores, *ACS Energy Letters* 3 (3) (2018) 618–621.
- [5] M. Debe, Electrocatalyst approaches and challenges for automotive fuel cells, *Nature* 486 (7401) (2012) 43–51.
- [6] M. Li, et al., Ultrafine jagged platinum nanowires enable ultrahigh mass activity for the oxygen reduction reaction, *Science* 354 (6318) (2016) 1414–1419, <https://doi.org/10.1126/science.aaf9050>.
- [7] S.-I. Choi, et al., Synthesis and characterization of 9 nm Pt–Ni octahedra with a record high activity of 3.3 A/mgPt for the oxygen reduction reaction, *Nano Lett.* 13 (7) (2013) 3420–3425.
- [8] B. Han, et al., Record activity and stability of dealloyed bimetallic catalysts for proton exchange membrane fuel cells, *Energy Environ. Sci.* 8 (1) (2015) 258–266.
- [9] Z. Wang, et al., Structurally ordered low-Pt intermetallic electrocatalysts toward durably high oxygen reduction reaction activity, *Adv. Funct. Mater.* 29 (35) (2019) 1902987.
- [10] D. Banham, S. Ye, Current status and future development of catalyst materials and catalyst layers for proton exchange membrane fuel cells: an industrial perspective, *ACS Energy Letters* 2 (3) (2017) 629–638.
- [11] L. Pan, et al., Current challenges related to the deployment of shape-controlled Pt alloy oxygen reduction reaction nanocatalysts into low Pt-loaded cathode layers of proton exchange membrane fuel cells, *Current Opinion in Electrochemistry* 18 (2019) 61–71.
- [12] V.R. Stamenkovic, N. Markovic, Tailored high performance low-PGM alloy cathode catalysts, Available from: https://www.hydrogen.energy.gov/pdfs/review16/fc140_stamenkovic_2016_o.pdf, 2016.
- [13] L. Chong, et al., Ultralow-loading platinum-cobalt fuel cell catalysts derived from imidazolate frameworks, *Science* (2018), eaau0630.
- [14] S. Khateeb, et al., Fuel cell performance of palladium-platinum core-shell electrocatalysts synthesized in gram-scale batches, *J. Electrochem. Soc.* 163 (7) (2016) F708–F713.
- [15] A. Kongkanand, M. Mathias, The priority and challenge of high-power performance of low-platinum proton-exchange membrane fuel cells, *J. Phys. Chem. Lett.* 7 (7) (2016) 1127–1137.
- [16] X. Ren, et al., Current progress of Pt and Pt-based electrocatalysts used for fuel cells, *Sustainable Energy & Fuels* 4 (1) (2020) 15–30.
- [17] X. Tian, et al., Advanced electrocatalysts for the oxygen reduction reaction in energy conversion technologies, *Joule* 4 (1) (2020) 45–68.
- [18] O. Gröger, H.A. Gasteiger, J.-P. Suchsland, Review—electromobility: batteries or fuel cells? *J. Electrochem. Soc.* 162 (14) (2015) A2605–A2622.
- [19] J. Bullion, Available from: <https://www.jmbullion.com/charts/platinum-price/>, 2019.
- [20] F. Barbir, PEM Fuel Cells: Theory and Practice, 2005. Elsevier Academic Press.
- [21] H.A. Gasteiger, et al., Activity benchmarks and requirements for Pt, Pt-alloy, and non-Pt oxygen reduction catalysts for PEMFCs, *Appl. Catal. B Environ.* 56 (1–2) (2005) 9–35.
- [22] M.L. Sattler, P.N. Ross, The surface structure of Pt crystallites supported on carbon black, *Ultramicroscopy* 20 (1–2) (1986) 21–28.
- [23] M. Shao, A. Peles, K. Shoemaker, Electrocatalysis on platinum nanoparticles: particle size effect on oxygen reduction reaction activity, *Nano Lett.* 11 (9) (2011) 3714–3719.
- [24] Z. Xu, et al., Effect of particle size on the activity and durability of the Pt/C electrocatalyst for proton exchange membrane fuel cells, *Appl. Catal. B Environ.* 111–112 (2012) 264–270.
- [25] S. Mukerjee, Particle size and structural effects in platinum electrocatalysis, *J. Appl. Electrochem.* 20 (4) (1990) 537–548.
- [26] P. Strasser, S. Kühn, Dealloyed Pt-based core-shell oxygen reduction electrocatalysts, *Nanomater. Energy* 29 (2016) 166–177.
- [27] P. Strasser, et al., Lattice-strain control of the activity in dealloyed core-shell fuel cell catalysts, *Nat. Chem.* 2 (6) (2010) 454–460.
- [28] M. Shao, et al., Recent advances in electrocatalysts for oxygen reduction reaction, *Chem Rev.* 2016.
- [29] T. Bligaard, J.K. Nørskov, Ligand effects in heterogeneous catalysis and electrochemistry, *Electrochim. Acta* 52 (18) (2007) 5512–5516.
- [30] A.R. Denton, N.W. Ashcroft, Vegard’s law, *Phys. Rev.* 43 (6) (1991) 3161–3164.
- [31] R.C. Cammarata, Surface and interface stress effects in thin films, *Prog. Surf. Sci.* 46 (1994) 1–38.
- [32] M. Escudero-Escribano, et al., Tuning the activity of Pt alloy electrocatalysts by means of the lanthanide contraction, *Science* 352 (6281) (2016) 73–76.
- [33] S. Mukerjee, J. McBreen, Effect of particle size on the electrocatalysis by carbon-supported Pt electrocatalysts: an in situ XAS investigation, Dedicated to Aleksandar R. Despic on the occasion of his seventieth birthday.1, *J. Electroanal. Chem.* 448 (2) (1998) 163–171.
- [34] D. Gohl, et al., Engineering stable electrocatalysts by synergistic stabilization between carbide cores and Pt shells, *Nat. Mater.* (2019).
- [35] S.-J. Hwang, et al., Supported core@shell electrocatalysts for fuel cells: close encounter with reality, *Sci. Rep.* 3 (2013) 1309.
- [36] S.-I. Choi, et al., Synthesis and characterization of Pd@Pt–Ni core-shell octahedra with high activity toward oxygen reduction, *ACS Nano* 8 (10) (2014) 10363–10371.
- [37] J. Wu, A. Gross, H. Yang, Shape and composition-controlled platinum alloy nanocrystals using carbon monoxide as reducing agent, *Nano Lett.* 11 (2) (2011) 798–802.
- [38] J. Zhang, et al., Synthesis and oxygen reduction activity of shape-controlled Pt₃Ni nanopolyhedra, *Nano Lett.* 10 (2) (2010) 638–644.
- [39] D. Li, et al., Functional links between Pt single crystal morphology and nanoparticles with different size and shape: the oxygen reduction reaction case, *Energy Environ. Sci.* 7 (12) (2014) 4061–4069.
- [40] R. Chattot, et al., Surface distortion as a unifying concept and descriptor in oxygen reduction reaction electrocatalysis, *Nat. Mater.* 17 (9) (2018) 827–833.
- [41] S. Sui, et al., A comprehensive review of Pt electrocatalysts for the oxygen reduction reaction: nanostructure, activity, mechanism and carbon support in PEM fuel cells, *J. Mater. Chem.* 5 (5) (2017) 1808–1825.
- [42] N. Markovic, H. Gasteiger, P.N. Ross, Kinetics of oxygen reduction on Pt(hkl) electrodes: implications for the crystallite size effect with supported Pt electrocatalysts, *J. Electrochem. Soc.* 144 (5) (1997) 1591–1597.
- [43] C.M. Zalitis, et al., Design principles for platinum nanoparticles catalysing electrochemical hydrogen evolution and oxidation reactions: edges are much more active than facets, *J. Mater. Chem.* 5 (44) (2017) 23328–23338.
- [44] J. Zeng, et al., In situ surface-enhanced Raman spectroscopic studies of nafion adsorption on Au and Pt electrodes, *Langmuir* 28 (1) (2012) 957–964.
- [45] K. Shinozaki, et al., Suppression of oxygen reduction reaction activity on Pt-based electrocatalysts from ionomer incorporation, *J. Power Sources* 325 (2016) 745–751.
- [46] T. Masuda, et al., Potential-dependent adsorption and desorption of perfluorosulfonated ionomer on a platinum electrode surface probed by electrochemical quartz crystal microbalance and atomic force microscopy, *J. Phys. Chem. C* 117 (30) (2013) 15704–15709.
- [47] D. Banham, et al., A review of the stability and durability of non-precious metal catalysts for the oxygen reduction reaction in proton exchange membrane fuel cells, *J. Power Sources* 285 (2015) 334–348, 0.
- [48] Y. Shao, et al., PGM-free cathode catalysts for PEM fuel cells: a mini-review on stability challenges, *Adv. Mater.* (2019) 1807615, 0(0).
- [49] D.C. Higgins, Z. Chen, Recent progress in non-precious metal catalysts for PEM fuel cell applications, *Can. J. Chem. Eng.* 91 (12) (2013) 1881–1895.
- [50] D. Malko, et al., The intriguing poison tolerance of non-precious metal oxygen reduction reaction (ORR) catalysts, *J. Mater. Chem.* 4 (1) (2016) 142–152.
- [51] T. Reshetenko, et al., Tolerance of non-platinum group metals cathodes proton exchange membrane fuel cells to air contaminants, *J. Power Sources* 324 (2016) 556–571.
- [52] J.-Y. Choi, et al., Is the rapid initial performance loss of Fe/N/C non precious metal catalysts due to micropore flooding? *Energy Environ. Sci.* 10 (1) (2017) 296–305.
- [53] W. Wang, et al., Recent insights into the oxygen-reduction electrocatalysis of Fe/N/C materials, *ACS Catal.* 9 (11) (2019) 10126–10141.
- [54] U. Martinez, et al., Progress in the development of Fe-based PGM-free electrocatalysts for the oxygen reduction reaction, *Adv. Mater.* 31 (31) (2019) 1806545.
- [55] H. Schulerburg, et al., Catalysts for the oxygen reduction from heat-treated iron (III) tetramethoxyphenylporphyrin Chloride: structure and stability of active sites, *J. Phys. Chem. B* 107 (34) (2003) 9034–9041.
- [56] M. Lefèvre, J.-P. Dodelet, Fe-based catalysts for the reduction of oxygen in polymer electrolyte membrane fuel cell conditions: determination of the amount of peroxide released during electroreduction and its influence on the stability of the catalysts, *Electrochim. Acta* 48 (19) (2003) 2749–2760.
- [57] B. Wang, Recent development of non-platinum catalysts for oxygen reduction reaction, *J. Power Sources* 152 (2005) 1–15, 0.
- [58] J. Herranz, et al., Unveiling N-protonation and anion-binding effects on Fe/N/C catalysts for O₂ reduction in proton-exchange-membrane fuel cells, *J. Phys. Chem. C* 115 (32) (2011) 16087–16097.
- [59] G. Zhang, et al., Is iron involved in the lack of stability of Fe/N/C electrocatalysts used to reduce oxygen at the cathode of PEM fuel cells? *Nanomater. Energy* 29 (2016) 111–125.
- [60] D. Banham, et al., Critical advancements in achieving high power and stable nonprecious metal catalyst-based MEAs for real-world proton exchange membrane fuel cell applications, *Science Advances* 4 (3) (2018) eaar7180.

- [61] F. Jaouen, et al., Heat-treated Fe/N/C catalysts for O₂ Electroreduction: are active sites hosted in micropores? *J. Phys. Chem. B* 110 (11) (2006) 5553–5558.
- [62] X. Li, G. Liu, B.N. Popov, Activity and stability of non-precious metal catalysts for oxygen reduction in acid and alkaline electrolytes, *J. Power Sources* 195 (19) (2010) 6373–6378.
- [63] T. Ikeda, et al., Carbon alloy catalysts: active sites for oxygen reduction reaction, *J. Phys. Chem. C* 112 (38) (2008) 14706–14709.
- [64] L. Xue, et al., Zigzag carbon as efficient and stable oxygen reduction electrocatalyst for proton exchange membrane fuel cells, *Nat. Commun.* 9 (1) (2018) 3819.
- [65] H.T. Chung, et al., Direct atomic-level insight into the active sites of a high-performance PGM-free ORR catalyst, *Science* 357 (6350) (2017) 479–484.
- [66] D. Banham, et al., Integrating PGM-free catalysts into catalyst layers and proton exchange membrane fuel cell devices, *Adv. Mater.* 31 (2019) 1804846.
- [67] B. Genorio, et al., Selective catalysts for the hydrogen oxidation and oxygen reduction reactions by patterning of platinum with calix[4]arene molecules, *Nat. Mater.* 9 (12) (2010) 998–1003.
- [68] S.-W. Yun, et al., Hydrogen oxidation-selective electrocatalysis by fine tuning of Pt ensemble sites to enhance the durability of automotive fuel cells, *ChemSusChem* 10 (3) (2017) 489–493.
- [69] N.M. Marković, P.N. Ross Jr., Surface science studies of model fuel cell electrocatalysts, *Surf. Sci. Rep.* 45 (4–6) (2002) 117–229.
- [70] C.H. Choi, et al., Tuning selectivity of electrochemical reactions by atomically dispersed platinum catalyst, *Nat. Commun.* 7 (2016) 10922.
- [71] S. Siahrostami, et al., Enabling direct H₂O₂ production through rational electrocatalyst design, *Nat. Mater.* 12 (12) (2013) 1137–1143.
- [72] A. Bruix, et al., Maximum noble-metal efficiency in catalytic materials: atomically dispersed surface platinum, *Angew Chem. Int. Ed. Engl.* 53 (39) (2014) 10525–10530.
- [73] X. Zeng, et al., Single-atom to single-atom grafting of Pt₁ onto Fe-N₄ center: Pt₁@Fe-N-C multifunctional electrocatalyst with significantly enhanced properties, *Advanced Energy Materials* 8 (1) (2018) 1701345.
- [74] V. Yarlagadda, et al., Preparation of PEMFC electrodes from milligram-amounts of catalyst powder, *J. Electrochem. Soc.* 164 (7) (2017) F845–F849.
- [75] J. Li, et al., The challenge of achieving a high density of Fe-based active sites in a highly graphitic carbon matrix, *Catalysts* 9 (2) (2019) 144.
- [76] F. Jaouen, et al., Toward platinum group metal-free catalysts for hydrogen/air proton-exchange membrane fuel cells, *Johnson Matthey Technology Review*, 2018.
- [77] S. Kinoshita, Anode overpotential at low Pt loadings for pure H₂, *ECS Transactions* 11 (1) (2007) 309–315.
- [78] H.A. Gasteiger, J.E. Panels, S.G. Yan, Dependence of PEM fuel cell performance on catalyst loading, *J. Power Sources* 127 (1–2) (2004) 162–171.
- [79] M. Secanell, et al., Optimal design of ultralow-platinum PEMFC anode electrodes, *J. Electrochem. Soc.* 155 (2) (2008) B125–B134.
- [80] B.K. Hong, et al., On the impact of water activity on reversal tolerant fuel cell anode performance and durability, *J. Power Sources* 328 (2016) 280–288.
- [81] S.J. Lee, et al., Electrocatalysis of CO tolerance in hydrogen oxidation reaction in PEM fuel cells, *Electrochim. Acta* 44 (19) (1999) 3283–3293.
- [82] G.A. Camara, et al., The CO poisoning mechanism of the hydrogen oxidation reaction in proton exchange membrane fuel cells, *J. Electrochem. Soc.* 149 (6) (2002).
- [83] J. Bockris, A. Reddy, M. Gamboa-Aldeco, *Modern Electrochemistry 2A Fundamentals of Electrode Processes*, second ed., Kluwer Academic/Plenum Publishers, New York, 2000.
- [84] W. Sheng, H.A. Gasteiger, Y. Shao-Horn, Hydrogen oxidation and evolution reaction kinetics on platinum: acid vs alkaline electrolytes, *J. Electrochem. Soc.* 157 (11) (2010) B1529–B1536.
- [85] J. Durst, et al., Hydrogen oxidation and evolution reaction (HOR/HER) on Pt electrodes in acid vs. Alkaline electrolytes: mechanism, activity and particle size effects, *ECS Transactions* 64 (3) (2014) 1069–1080.
- [86] T.A. Greszler, D. Caulk, P. Sinha, The impact of platinum loading on oxygen transport resistance, *J. Electrochem. Soc.* 159 (12) (2012) F831–F840.
- [87] K. Sakai, et al., Analysis of reactant gas transport in catalyst layers; effect of Pt-loadings, *ECS Transactions* 25 (1) (2009) 1193–1201.
- [88] N. Nonoyama, et al., Analysis of oxygen-transport diffusion resistance in proton-exchange-membrane fuel cells, *J. Electrochem. Soc.* 158 (4) (2011) B416–B423.
- [89] M.K. Debe, Effect of electrode surface area distribution on high current density performance of PEM fuel cells, *J. Electrochem. Soc.* 159 (1) (2011) B53–B66.
- [90] K. Kudo, Y. Morimoto, Analysis of oxygen transport resistance of nafion thin film on Pt electrode, *ECS Transactions* 50 (2) (2013) 1487–1494.
- [91] R. Jinnouchi, et al., Molecular dynamics simulations on O₂ permeation through nafion ionomer on platinum surface, *Electrochim. Acta* 188 (2016) 767–776.
- [92] P. Zihrl, et al., Voltage cycling induced losses in electrochemically active surface area and in H₂/air-performance of PEM fuel cells, *J. Electrochem. Soc.* 163 (6) (2016) F492–F498.
- [93] A. Kusoglu, A.Z. Weber, New insights into perfluorinated sulfonic-acid ionomers, *Chem. Rev.* 117 (3) (2017) 987–1104.
- [94] H. Liu, W.K. Epting, S. Litster, Gas transport resistance in polymer electrolyte thin films on oxygen reduction reaction catalysts, *Langmuir* (2015).
- [95] T. Muzaffar, T. Kadyk, M. Eikerling, Tipping water balance and the Pt loading effect in polymer electrolyte fuel cells: a model-based analysis, *Sustainable Energy & Fuels* 2 (6) (2018) 1189–1196.
- [96] G.S. Harzer, et al., Tailoring catalyst morphology towards high performance for low Pt loaded PEMFC cathodes, *J. Electrochem. Soc.* 165 (10) (2018) F770–F779.
- [97] Y.-C. Park, et al., Effects of carbon supports on Pt distribution, ionomer coverage and cathode performance for polymer electrolyte fuel cells, *J. Power Sources* 315 (2016) 179–191.
- [98] E.P. Ambrosio, et al., Ordered mesoporous carbons as catalyst support for PEM fuel cells, *Fuel Cell* 9 (3) (2009) 197–200.
- [99] N.P. Lebedeva, A.S. Booi, G.J. Janssen, Cathodes for proton-exchange-membrane fuel cells based on ordered mesoporous carbon supports, *ECS Transactions* 16 (2) (2008) 2083–2092.
- [100] D. Banham, et al., Effect of carbon support nanostructure on the oxygen reduction activity of Pt/C catalysts, *J. Mater. Chem.* 1 (8) (2013) 2812–2820.
- [101] D. Banham, et al., First time investigation of Pt nanocatalysts deposited inside carbon mesopores of controlled length and diameter, *J. Mater. Chem.* 22 (15) (2012) 7164–7171.
- [102] D. Banham, et al., Effect of Pt-loaded carbon support nanostructure on oxygen reduction catalysis, *J. Power Sources* 196 (13) (2011) 5438–5445.
- [103] S.H. Joo, et al., Ordered nanoporous arrays of carbon supporting high dispersions of platinum nanoparticles, *Nature* 412 (6843) (2001) 169.
- [104] E. Ambrosio, et al., Mesoporous carbons as low temperature fuel cell platinum catalyst supports, *J. Appl. Electrochem.* 38 (7) (2008) 1019–1027.
- [105] J. Zeng, et al., Method for preparing highly dispersed Pt catalysts on mesoporous carbon support, *J. Mater. Sci.* 42 (17) (2007) 7191–7197.
- [106] J.Y. Cheon, et al., Ordered mesoporous porphyrinic carbons with very high electrocatalytic activity for the oxygen reduction reaction, *Sci. Rep.* 3 (2013).
- [107] H.G. Petrow, R.J. Allen, *Catalytic Platinum Metal Particles on a Substrate and Method of Preparing the Catalyst*, 1976.
- [108] P. Serp, J.L. Figueiredo, *Carbon Materials for Catalysis*, John Wiley & Sons, Inc, Hoboken, New Jersey, 2008.
- [109] K.C. Neyerlin, et al., Cathode catalyst utilization for the ORR in a PEMFC, *J. Electrochem. Soc.* 154 (2) (2007) B279.
- [110] E. Michael, Modeling of catalyst layer performance. *Polymer Electrolyte Fuel Cells*, CRC Press, 2014, pp. 263–364.
- [111] T. Ito, et al., Three-dimensional spatial distributions of Pt catalyst nanoparticles on carbon substrates in polymer electrolyte fuel cells, *Electrochemistry* 79 (5) (2011) 374–376.
- [112] M. Carmo, M. Linardi, J.G.R. Poco, Characterization of nitric acid functionalized carbon black and its evaluation as electrocatalyst support for direct methanol fuel cell applications, *Appl. Catal. Gen.* 355 (1) (2009) 132–138.
- [113] A. Guha, et al., Surface-modified carbons as platinum catalyst support for PEM fuel cells, *Carbon* 45 (7) (2007) 1506–1517.
- [114] Y. Chen, et al., Nitrogen doping effects on carbon nanotubes and the origin of the enhanced electrocatalytic activity of supported Pt for proton-exchange membrane fuel cells, *J. Phys. Chem. C* 115 (9) (2011) 3769–3776.
- [115] H. Schmies, et al., Impact of carbon support functionalization on the electrochemical stability of Pt fuel cell catalysts, *Chem. Mater.* 30 (20) (2018) 7287–7295.
- [116] Z. Qiao, et al., 3D porous graphitic nanocarbon for enhancing the performance and durability of Pt catalysts: a balance between graphitization and hierarchical porosity, *Energy & Environmental Science*, 2019.
- [117] A. Orfanidi, et al., The key to high performance low Pt loaded electrodes, *J. Electrochem. Soc.* 164 (4) (2017) F418–F426.
- [118] S. Ott, et al., Ionomer distribution control in porous carbon-supported catalyst layers for high-power and low Pt-loaded proton exchange membrane fuel cells, *Nat. Mater.* 19 (1) (2020) 77–85.
- [119] J.X. Wang, N.M. Markovic, R.R. Adzic, Kinetic analysis of oxygen reduction on Pt (111) in acid solutions: intrinsic kinetic parameters and anion adsorption effects, *J. Phys. Chem. B* 108 (13) (2004) 4127–4133.
- [120] D. Banham, et al., Bimodal, templated mesoporous carbons for capacitor applications, *Carbon* 48 (4) (2010) 1056–1063.
- [121] T. Jiang, et al., A novel sulfur-nitrogen dual doped ordered mesoporous carbon electrocatalyst for efficient oxygen reduction reaction, *Appl. Catal. B Environ.* 189 (2016) 1–11.
- [122] W. Li, D. Zhao, An overview of the synthesis of ordered mesoporous materials, *Chem. Commun.* 49 (10) (2013) 943–946.
- [123] W. Li, et al., Ordered mesoporous materials based on interfacial assembly and engineering, *Adv. Mater.* 25 (37) (2013) 5129–5152.
- [124] W. Li, J. Liu, D. Zhao, Mesoporous materials for energy conversion and storage devices, *Nature Reviews Materials* 1 (6) (2016) 16023.
- [125] Y. Meng, et al., Ordered mesoporous polymers and homologous carbon frameworks: amphiphilic surfactant templating and direct transformation, *Angew. Chem. Int. Ed.* 44 (43) (2005) 7053–7059.
- [126] S. Feng, et al., Hydrothermal synthesis of ordered mesoporous carbons from a biomass-derived precursor for electrochemical capacitors, *Nanoscale* 6 (24) (2014) 14657–14661.
- [127] Y. Zhai, et al., Carbon materials for chemical capacitive energy storage, *Adv. Mater.* 23 (42) (2011) 4828–4850.
- [128] D. Banham, et al., Novel mesoporous carbon supports for PEMFC catalysts, *Catalysts* 5 (3) (2015) 1046.
- [129] E.P. Ambrosio, et al., Platinum catalyst supported on mesoporous carbon for PEMFC, *Int. J. Hydrogen Energy* 33 (12) (2008) 3142–3145.
- [130] Z. Li, M. Jaroniec, Colloidal imprinting: a novel approach to the synthesis of mesoporous carbons, *J. Am. Chem. Soc.* 123 (37) (2001) 9208–9209.
- [131] G.S. Chai, et al., Ordered porous carbons with tunable pore sizes as catalyst supports in direct methanol fuel cell, *J. Phys. Chem. B* 108 (22) (2004) 7074–7079.
- [132] A.A. Zakhidov, et al., Carbon structures with three-dimensional periodicity at optical wavelengths, *Science* 282 (5390) (1998) 897–901.

- [133] S. Jun, et al., Synthesis of new, nanoporous carbon with hexagonally ordered mesostructure, *J. Am. Chem. Soc.* 122 (43) (2000) 10712–10713.
- [134] A. Stein, F. Li, N.R. Denny, Morphological control in colloidal crystal templating of inverse opals, hierarchical structures, and shaped particles, *Chem. Mater.* 20 (3) (2007) 649–666.
- [135] J.B.K. Joo, P. Kim, J. Yi, Preparation of Pt supported on mesoporous carbons for the reduction of oxygen in polymer electrolyte membrane fuel cell (PEMFC), *J. Electroceram.* 17 (2) (2006) 713–718.
- [136] B. Fang, et al., Ordered hierarchical nanostructured carbon as a highly efficient cathode catalyst support in proton exchange membrane fuel cell, *Chem. Mater.* 21 (5) (2009) 789–796.
- [137] B. Fang, J.H. Kim, J.-S. Yu, Colloid-imprinted carbon with superb nanostructure as an efficient cathode electrocatalyst support in proton exchange membrane fuel cell, *Electrochem. Commun.* 10 (4) (2008) 659–662.
- [138] K. Pei, et al., Oxygen reduction activity dependence on the mesoporous structure of imprinted carbon supports, *Electrochem. Commun.* 12 (11) (2010) 1666–1669.
- [139] K.P. Gierszal, et al., Adsorption and structural properties of mesoporous carbons obtained from mesophase pitch and phenol-formaldehyde carbon precursors using porous templates prepared from colloidal silica, *J. Mater. Chem.* 16 (2006) 2819–2823.
- [140] T.D. Gierke, G.E. Munn, F.C. Wilson, *The Morphology in nafion® perfluorinated membrane products, as determined by wide- and small- angle X-ray studies*, *J. Polym. Sci. Polym. Phys. Ed* 19 (1981) 1687–1704.
- [141] E. Antolini, Carbon supports for low-temperature fuel cell catalysts, *Appl. Catal. B Environ.* 88 (1–2) (2009) 1–24.
- [142] S.H. Hur, J.-N. Park, Graphene and its application in fuel cell catalysis: a review, *Asia Pac. J. Chem. Eng.* 8 (2) (2013) 218–233.
- [143] M.A. Hoque, et al., Optimization of sulfur-doped graphene as an emerging platinum nanowires support for oxygen reduction reaction, *Nanomater. Energy* 19 (2016) 27–38.
- [144] D. Higgins, et al., Development and simulation of sulfur-doped graphene supported platinum with exemplary stability and activity towards oxygen reduction, *Adv. Funct. Mater.* 24 (27) (2014) 4325–4336.
- [145] J. Li, et al., N dual-doped graphene-like carbon nanosheets as efficient oxygen reduction reaction electrocatalysts, *ACS Appl. Mater. Interfaces* 9 (1) (2017) 398–405.
- [146] D. Guo, et al., Active sites of nitrogen-doped carbon materials for oxygen reduction reaction clarified using model catalysts, *Science* 351 (6271) (2016) 361.
- [147] Q. Shi, et al., Sulfur and nitrogen co-doped carbon nanotubes for enhancing electrochemical oxygen reduction activity in acidic and alkaline media, *J. Mater. Chem.* 1 (47) (2013) 14853–14857.
- [148] K. Gong, et al., Nitrogen-doped carbon nanotube Arrays with high electrocatalytic activity for oxygen reduction, *Science* 323 (5915) (2009) 760–764.
- [149] J.N. Tiwari, et al., Stable platinum nanoclusters on genomic DNA–graphene oxide with a high oxygen reduction reaction activity, *Nat. Commun.* 4 (1) (2013) 2221.
- [150] Q. Wang, et al., Structure and performance of different types of agglomerates in cathode catalyst layers of PEM fuel cells, *J. Electroanal. Chem.* 573 (1) (2004) 61–69.
- [151] Y. Jiao, et al., Highly ordered mesoporous few-layer graphene frameworks enabled by Fe₃O₄ nanocrystal superlattices, *Angew. Chem. Int. Ed.* 54 (19) (2015) 5727–5731.
- [152] L. Gubler, S.M. Dockheer, W.H. Koppenol, Radical (HO•, H• and HOO•) formation and ionomer degradation in polymer electrolyte fuel cells, *J. Electrochem. Soc.* 158 (7) (2011) B755–B769.
- [153] H. Yu, et al., Designed synthesis of ordered mesoporous graphene spheres from colloidal nanocrystals and their application as a platform for high-performance lithium-ion battery composite electrodes, *Nano Research* 9 (12) (2016) 3757–3771.
- [154] L. Ji, et al., Free-standing, ordered mesoporous few-layer graphene framework films derived from nanocrystal superlattices self-assembled at the solid– or liquid–air interface, *Chem. Mater.* 28 (11) (2016) 3823–3830.
- [155] T. Li, et al., Self-assembled nanoparticle supertubes as robust platform for revealing long-term, *Multiscale Lithiation Evolution. Matter* 1 (4) (2019) 976–987.
- [156] J. Zheng, et al., Elaborately designed micro–mesoporous graphitic carbon spheres as efficient polysulfide reservoir for lithium–sulfur batteries, *ACS Energy Letters* 2 (5) (2017) 1105–1114.
- [157] P. Qiu, et al., Spherical mesoporous materials from single to multilevel architectures, *Acc. Chem. Res.* 52 (10) (2019) 2928–2938.
- [158] L. Peng, et al., Versatile nanoemulsion assembly approach to synthesize functional mesoporous carbon nanospheres with tunable pore sizes and architectures, *J. Am. Chem. Soc.* 141 (17) (2019) 7073–7080.
- [159] X. Zhu, et al., Synthesis of carbon nanotubes@mesoporous carbon core–shell structured electrocatalysts via a molecule-mediated interfacial co-assembly strategy, *J. Mater. Chem.* 7 (15) (2019) 8975–8983.
- [160] K. Shinozaki, et al., Oxygen reduction reaction measurements on platinum electrocatalysts utilizing rotating disk electrode technique, *J. Electrochem. Soc.* 162 (12) (2015) F1384–F1396.
- [161] S. Martens, et al., A comparison of rotating disc electrode, floating electrode technique and membrane electrode assembly measurements for catalyst testing, *J. Power Sources* 392 (2018) 274–284.
- [162] A. Riese, et al., Accelerated stress testing by rotating disk electrode for carbon corrosion in fuel cell catalyst supports, *J. Electrochem. Soc.* 162 (7) (2015) F783–F788.